J. Plasma Physics (1999), *vol.* 61, *part* 3, *pp.* 507–541. Printed in the United Kingdom

Parametric investigation of self-similar decay laws in MHD turbulent flows*

S. GALTIER,[1] E. ZIENICKE,[1,2] H. POLITANO[1] and A. POUQUET[1]

[1] Observatoire de la Côte d'Azur, CNRS UMR 6529, BP 4229, 06304 Nice Cedex 4, France

[2] Forschungszentrum Rossendorf, Haus 101.1, Postfach 510119D-01314 Dresden, Germany

(Received 22 October 1998)

An investigation of the decay laws of energy and of higher moments of the Elsässer fields $\mathbf{z}^{\pm} = \mathbf{v} \pm \mathbf{b}$ in the self-similar regime of magnetohydrodynamic (MHD) turbulence is presented, using phenomenological models as well as two-dimensional numerical simulations with periodic boundary conditions and up to 2048^2 grid points. The results are compared with the generalization of the parameter-free model derived by Galtier et al. [*Phys. Rev. Lett.* **79**, 2807 (1997)], which takes into account the slowing down of the dynamics due to the propagation of Alfvén waves. The new model developed here allows for a study in terms of one parameter governing the wavenumber dependence of the energy spectrum at scales of the order of (and larger than) the integral scale of the flow. The one-dimensional compressible case is also dealt with in two of its simplest configurations. Computations are performed for a standard Laplacian diffusion as well as with a hyperdiffusive algorithm. The results are sensitive to the amount of correlation between the velocity and the magnetic field, but rather insensitive to all other parameters such as the initial ratio of kinetic to magnetic energy or the presence or absence of a uniform component of the magnetic field. In all cases, the decay is significantly slower than for neutral fluids in a way that favours for MHD flows the phenomenology of Iroshnikov [*Soviet Astron.* **7**, 566 (1963)] and Kraichnan [*Phys. Fluids* **8**, 1385 (1965)] as opposed to that of Kolmogorov [*Dokl. Akad. Nauk. SSSR* **31**, 538 (1941)]. The temporal evolution of q-moments of the generalized vorticities $\langle |\boldsymbol{\omega}^{\pm}|^q \rangle = \langle |\boldsymbol{\omega} \pm \mathbf{j}|^q \rangle$ up to order $q = 10$ is also given, and is compared with the prediction of the model. Less agreement obtains as q grows – a fact probably due to intermittency and the development of coherent structures in the form of eddies, and of vorticity and current sheets.

**Dedication*. We should like to dedicate this work to Professor David Montgomery on the occasion of his sixty-plus birthday, since one of us (A.P.) so miserably failed to meet the deadline for the special issue on the occasion of his sixtieth birthday. Our full apologies to him, but the research presented here grew larger and much more slowly than planned initially. His long-standing keen interest in all the issues concerning MHD turbulence and in the relevance of the Kraichnan approach to describe nonlinear interactions in MHD is behind the motivation for this work.

1. Introduction

It is well known that in a turbulent flow nonlinearities lead to an enhanced decay of energy – a phenomenon generally covered by the concept of eddy viscosity, and, in MHD, eddy resistivity as well. A formulation of these transport coefficients may be obtained in the context of turbulent closure schemes, and indicates that energy decays at a substantial rate even for very high Reynolds numbers (for a review, see e.g. Pouquet 1993). It is then of interest to ask what are the parameters that govern such a decay, and at what rate does energy decay: is the rate set by the actual value of the Reynolds number, or does it depend on other parameters, such as characteristic velocity, magnetic field and length scales? Note that, it is often stated that, in view of the very high Reynolds numbers in astrophysical and geophysical flows, no source of energy is needed to maintain such flows, the energy being almost exactly conserved. On the other hand, if decay takes place, irrespective of the value of the Reynolds number, a source of energy must be found for these flows. In the case of the solar wind, the plasma is clearly accelerated in the wake of a flare, although it is not yet obvious how to reach the velocities for the wind at some 800 km s^{-1}. The problem of an energy source is still open for the supersonic flows observed in the interstellar medium, where one can consider galactic shear, ionization winds and supernova blast waves.

A full kinetic approach should be taken in order to study the problem of decay of kinetic and magnetic energy in natural plasmas. However, for velocities substantially smaller than the speed of light and at large spatial and temporal scales, the MHD approximation is valid. Since the energy is contained in the large scales, and its decay is governed by the largest scales of the flow (see below), it may then be argued that, at least in a first approach, the MHD approximation will suffice.

In this paper, we investigate the self-similar decay of energy with time in conducting flows. The case of low magnetic Reynolds number, which is relevant to many laboratory experiments, has been examined by Moffatt (1967) (see also Davidson 1995), whereas one deals here rather with high kinetic and magnetic Reynolds numbers, which are relevant in many astrophysical flows, for example in the solar wind or the interstellar medium as mentioned above.

The final period of decay – for $t > t_D$, where t_D is the characteristic dissipation time of the large scales – is dominated by the viscosity ν and the magnetic diffusivity η. We assume here that $\nu \sim \eta$. This is, in general, inconsistent with the physics of astro-geophysical flows. However, we rely on the argument that a unit magnetic Prandtl number may be justified by a renormalization group analysis (Fournier et al. 1982), through which it is shown that, for homogeneous isotropic and incompressible MHD flows, the magnetic Prandtl number tends to a value close to unity. Then, one deduces, in the isotropic case, a decay law of turbulent energy $E^V(t) \sim t^{-5/2}$ in three dimensions (see e.g. Monin and Yaglom 1975) from the exponential decay of the energy spectrum in Fourier space:

$$E^V(k,t) \sim \exp(-2\nu k^2 t),$$

with

$$E^V = \tfrac{1}{2}\langle \mathbf{v}^2 \rangle = \int E^V(k)\, dk.$$

One assumes that there exists an interval of time $t_* < t < t_D$, after the initial development of small scales through nonlinear interactions and before the final period of decay, during which the energy decreases in a self-similar manner. Then, in the neutral fluid case, from a phenomenological argument following that of Kolmogorov (1941) (hereinafter referred to as K41), it can be deduced that $E^V(t) \sim (t-t_*)^{-10/7}$ in the standard case (see below), where t_* is taken as the time at which the dissipation $\mathscr{D}$ reaches its first maximum. Experiments are roughly in agreement with such an evaluation (Comte-Bellot and Corrsin 1966; Warhaft and Lumley 1978), although error bars are large. However, in a set-up in liquid helium II in which the integral scale of the flow is fixed by the boundary conditions, one finds $E^V(t) \sim (t-t_*)^{-2}$ (Smith et al. 1993; Lohse 1994). Such a rapid decay had also been observed numerically at a moderate Reynolds number (G. S. Patterson, unpublished data; see also Kerr 1981). In fact, this t^{-2} law can be recovered in the spirit of K41, with a slight change in the analysis. Indeed, the derivation of Kolmogorov uses the Loitsianskii 'invariant'

$$\sim v_{\mathrm{rms}}^2 \int_0^\infty r^4 f(r)\, dr,$$

where $f(r)$ is the longitudinal correlation function of the velocity. This assumption is known to be not universally valid, in particular because of the non-locality of the pressure, and in fact is not needed. It can be replaced by stipulating that a spectrum of the form

$$E^V(k) \sim k^s \tag{1}$$

up to $k_0 = 2\pi/l_0$ persists in time, l_0 being identified with the integral scale of the flow defined as

$$\frac{\int k^{-1} E^V(k)\, dk}{E^V}.$$

Isotropy is assumed and $1 \leqslant s \leqslant 4$ (see Monin and Yaglom 1975). In the Loitsianskii framework with an eddy noise due to the beating effect of small-scale eddies on large-scale ones, a k^{D+1} spectrum obtains in the large scales, where D is the space dimension. On the other hand, in the case of equipartition of individual Fourier modes (Saffman 1967a, b; Chasnov 1995) linked to the less-restrictive assumption of convergence of moments of the vorticity (as opposed to velocity), one has $s = D-1$, as in the compressible case. This may also be relevant when anisotropy develops in the flow (see also Garnier et al. 1981), as, for example, in the presence of an external uniform magnetic field, and with gravity or rotation.

We recall here for completeness the derivation of the K41 result and its generalization to variable s (see e.g. Lesieur and Schertzer 1978). The analysis is restricted to homogeneous, isotropic and incompressible turbulence. All three assumptions are an idealization of realistic flows, and as such this approach is academic. It is of interest, then, that laboratory flows may indeed behave in a way sufficiently close to the predictions of the analysis given below. The reason may be that, sufficiently far from boundaries, and at small scales, these assumptions are recovered in a statistical sense. Since the same may be said for conducting flows, we shall also restrict the analysis to the homogeneous,

isotropic and incompressible case. However, compressibility will be discussed in Sec. 3.

In the large scales, assume then that $E^V(k) \sim k^s$ up to l_0, after which the inertial range begins. This large-scale power-law spectrum dominates the total energy, which can thus be evaluated as $E^V \sim l_0^{-(s+1)}$. Both l_0 and E^V are assumed to be self-similar in time, namely

$$\langle \mathbf{v}^2 \rangle(t) \sim (t-t_*)^{-\alpha_s}, \qquad l_0(t) \sim (t-t_*)^{\beta_s},$$

the final exponential phase of decay not being considered, as stated above. Thus $\alpha_s = \beta_s(s+1)$, since $v^2 l_0^{s+1} = \text{const}$ (denoting for brevity $v^2 = \langle \mathbf{v}^2 \rangle$). Differentiating this last expression and introducing the energy transfer and decay rate $\epsilon_V \equiv -\dot{E}^V$ leads to $1-\beta_s = \frac{1}{2}\alpha_s$, where the Kolmogorov relationship $\epsilon_V \sim v^3/l_0$ has been used. The decay laws thus obtain with

$$\alpha_s = \frac{2(s+1)}{s+3}, \qquad \beta_s = \frac{2}{s+3}. \tag{2}$$

When $s = D+1 = 4$, corresponding to the back-scattering that emerges naturally in a freely decaying isotropic three-dimensional turbulent flow – unless constraints (e.g. at the boundaries) prevent it – the Kolmogorov law $E^V(t) \sim (t-t_*)^{-10/7}$ is immediately recovered. For the case of equipartition ($s = 2$), one recovers the prediction of Saffman (1967a, b) with $\alpha_2 = \frac{6}{5}$; this latter law is verified well in the case of the computations performed by Chasnov (1995). Note also that when the assumption of incompressibility is dropped, the spectrum for $k \to 0$ scales as $s = D-1$, leading to a *lower* decay rate than for the equivalent case of incompressible flow, the large-scale buffer storage of energy being more important. On the other hand, for a time-independent integral scale (a case that can be simply mimicked by taking the limit $s \to \infty$), one then recovers both the numerical results of Kerr (1981) and the experimental result of Smith et al. (1993), namely $\alpha_\infty = 2$.

If we now define the Reynolds number as

$$R = \frac{l_0 (2E^V)^{1/2}}{\nu},$$

we obtain

$$R(t) \sim (t-t_*)^{-r_s}, \qquad \text{with} \quad r_s = \frac{s-1}{3+s}.$$

Again for $s \to \infty$, this leads to $R(t) \sim (t-t_*)^{-1}$, in agreement with the results of Smith et al. (1993) (see also Lohse (1994) for a derivation of this law using the relationship $\epsilon_V \sim v^3/l_0$). Similarly, the Kolmogorov dissipation wavenumber $k_D \sim (\epsilon_V/\nu^3)^{1/4}$ decays as $(t-t_*)^{-\kappa_s}$, with $4(s+3)\kappa_s = 3s+5$. Finally, note that since, dimensionally, the energy dissipation rate ϵ_V scales as $E^V(t)/t$, it will itself decay as $\epsilon_V(t) \sim (t-t_*)^{-(\alpha_s+1)}$.

A similar analysis, but for MHD flows, is now performed in the next section.

2. Slowing-down of energy decay in MHD flows

2.1. Equations

The MHD equations for incompressible conducting flows read

$$(\partial_t + \mathbf{v}\cdot\boldsymbol{\nabla})\,\mathbf{v} = -\boldsymbol{\nabla} P_* + \nu \nabla^2 \mathbf{v} + \mathbf{b}\cdot\boldsymbol{\nabla}\mathbf{b}, \tag{3}$$

$$(\partial_t + \mathbf{v}\cdot\boldsymbol{\nabla})\,\mathbf{b} = \mathbf{b}\cdot\boldsymbol{\nabla}\mathbf{v} + \eta \nabla^2 \mathbf{b}, \tag{4}$$

where $\mathbf{b}$ is the magnetic induction and P_* the total pressure, and with $\boldsymbol{\nabla}\cdot\mathbf{v} = 0$ and $\boldsymbol{\nabla}\cdot\mathbf{b} = 0$. The uniform density is taken equal to unity.

For such a system, the weakening of the energy transfer to small scales because of the presence of Alfvén waves as postulated by Iroshnikov (1963) and Kraichnan (1965) leads to a total energy spectrum

$$E^T(k) \sim (\epsilon_T B_0)^{1/2} k^{-3/2}$$

(hereinafter referred to as the IK spectrum); where $\epsilon_T = -\dot{E}^T(t)$ is now the total (kinetic plus magnetic) energy transfer rate and B_0 is a large-scale, not necessarily uniform, magnetic field. The temporal decay laws within the framework of the IK phenomenology are obtained in a straightforward manner. The derivation follows closely that of K41, but taking into account the fact that the characteristic time of transfer of energy to small scales is longer than for a neutral fluid. We consider here the $E^{\pm}(k)$ energy spectra associated with the Elsässer fields $\mathbf{z}^{\pm} = \mathbf{v} \pm \mathbf{b}$. The amount of correlation between the velocity and the magnetic field is assumed negligible, and hence the Elsässer eddies at scale l behave in identical ways $z_l^+ \sim z_l^- \sim z_l$ (see, however, the Appendix concerning this point). As before, we assume a spectral behaviour $E^{\pm}(k) \sim k^s$ at low wavenumber, and a self-similar evolution for the energy and the integral scale:

$$z^2(t) \sim (t - t_*)^{-\alpha_{g,s}}, \qquad l_B(t) \sim (t - t_*)^{\beta_{g,s}}, \tag{5}$$

with $l_B \equiv l_B^{\pm}(t)$ and $z^2 \equiv \langle \mathbf{z}^{\pm^2} \rangle(t)$.

One can note further that the presence of inverse cascades in MHD (for a review, see Pouquet 1993) does not invalidate the assumption $E^{\pm}(k) \sim k^s$, provided that the boundary due to the finite size of the system is sufficiently far from the energy-containing scale from which this inverse cascade originates; this implies that the analysis presented here is only valid for moderate times. An estimate of the time needed to reach a given scale in an inverse cascade is readily obtained (see e.g. Pouquet 1978, 1993), by means of a dimensional analysis à la Kolmogorov, which yields the power-law spectrum followed by the $\mathscr{L}_2$ norm of the invariant field; the argument can be easily extended to the 3D case. In the limit of infinite Reynolds number, these two ranges of scales are well separated: that for which an inverse cascade is going on (the squared magnetic potential in two dimensions, and the magnetic helicity in three dimensions), and that for which the direct cascade of energy to small scales takes place. In that spirit, this inverse transfer due to the presence of a magnetic invariant is ignored in the present analysis. For decay laws of the energy and integral scale based directly on the effect of such inverse cascades, see Hatori (1984) for the case of neutral fluids and Biskamp (1994) for MHD. From a numerical point of view, however, the separation of domains is not of course so straightforward.

2.2. Derivation of a general model

In order to model an energy transfer to small scales with arbitrary scaling, we generalize the IK phenomenology by replacing the K41 expression for the energy transfer by

$$\epsilon_g = \frac{z^2}{\tau_{\mathrm{tr}}} = \frac{z^g}{l_B B_0^{(g-3)}}, \tag{6}$$

with $g \geqslant 3$, $\epsilon_g = -\dot{E}^{\pm}(t)$, and assuming weak velocity–magnetic-field corre-

lations. In (6), the transfer time $\tau_{\rm tr}$ has been evaluated with a simple rule, namely

$$\tau_{\rm tr} = \tau_{NL}\left(\frac{\tau_{NL}}{\tau_A}\right)^{g-3}, \tag{7}$$

where $\tau_{NL} = l_B/z_{l_B}$ and $\tau_A = l_B/B_0$ are respectively the turnover and Alfvén times at scale l_B (see also Politano and Pouquet 1995). In such an expression, $g = 3$ corresponds in fact to K41 (with $z \equiv v$), and $g = 4$ to the standard IK case (Galtier et al. 1997). A more significant slowing-down of transfer to small scales as advocated by Cattaneo and Vainshtein (1991) and Vainshtein and Cattaneo (1992) can be modelled in this framework with $g > 4$.

An overall dependence on the magnetic Reynolds number $E^{T\pm}(t) \sim R_M^{(\cdot)}(t-t_*)^{-\alpha_{g,s}}$ (with '$(\cdot)$' an open parameter) could be also advocated, but present-day numerical simulations do not allow for a sufficient scan of Reynolds number for this effect to be observed. This point is thus outside the scope of the present analysis, where we assume no dependence on Reynolds number, provided it be sufficiently large to allow for a long enough self-similar temporal decay range.

The generalization to $g \neq 3$ of the decay law for MHD is straightforward. With $\alpha_{g,s} = (s+1)\beta_{g,s}$ again, and using (6) and (7), one finds

$$\beta_{g,s} = \frac{2}{f(g)}, \quad f(g) = g(s+1) = 2s, \quad \alpha_{g,s} = (s+1)\,\beta_{g,s}, \tag{8}$$

with $f(g) \neq 0$, since $g \geqslant 3$ and $s \geqslant 1$. The special case of a constant integral scale ($\beta_{g,s} = 0$) can be recovered, as stated before, on letting $s \to \infty$. Note that for all $g \neq 3$, the resulting decay is less efficient than for K41 (for $s \geqslant 1$), a fact consistent with the IK phenomenology. The model with $s = D+1$ and $g = 4$ was derived already by Galtier et al. (1997), hereinafter referred to as the standard MHD case, and reads

$$\beta_{4,D+1} = \frac{1}{D+3}, \quad \alpha_{4,D+1} = \frac{D+2}{D+3}. \tag{9}$$

The values of $\alpha_{g,s}$ and $\beta_{g,s}$ given in (8) depend weakly on the parameter s. They may not be distinguishable in numerical integrations for which the large-scale spectrum k^s is not perfectly controlled (e.g. because of inverse transfer). For example, in the numerical integration of the 2D Navier–Stokes equations, a choice of $k_0/k_{\rm min} = 300$ was made (Chasnov 1995), where $k_{\rm min}$ corresponds to the largest scale of the flow, in order to obtain a clear scale separation between the k^s range and the inverse cascade range, at the expense of lowering the Reynolds number substantially.

The decay law of the Reynolds number follows immediately:

$$R_M(t) \sim (t-t_*)^{-r_{g,s}}, \quad \text{with} \quad r_{g,s} = \frac{s-1}{f(g)}.$$

Similarly as for the pure fluid case, the law for the temporal evolution of the dissipation wavenumber $k_{D,IK} = (z^4/lB_0^2\nu^2)^{1/3}$ for $\nu \sim \eta$ (see e.g. Pouquet 1993) can be deduced as well:

$$k_{D,IK}(t) \sim (t-t_*)^{-\kappa_{B,s}}, \quad \text{with} \quad 3f(4)\kappa_{B,s} = 2(2s+3),$$

specifying for simplicity $g = 4$. Finally, in the case of a constant integral scale, corresponding in our model to $\beta_s = 0$, we simply have

$$\alpha_{g,\infty} = \frac{2}{g-2}, \qquad r_{g,\infty} = \frac{1}{g-2};$$

the decay is thus fastest both for fluids and MHD than for any other value of s. This is a somewhat unfavourable numerical situation when studying decaying turbulence, since the turbulent self-similar regime only holds for times during which the Reynolds number remains substantially larger than unity.

It has been shown in the framework of two-point closures of turbulence that there may be a correction to the Kolmogorov $\frac{10}{7}$ temporal law (Lesieur and Schertzer 1978) for $s = 4$. Similar closures have been developed in MHD (Pouquet 1993), and could be used to compute the corresponding corrective factor. However, this factor is small for neutral fluids, since it changes the $(t-t_*)^{-10/7}$ law into a $(t-t_*)^{-1.36}$ law. If such is the case in MHD as well, it is unlikely that such a modification could be discernable in present-day direct numerical simulations, although it could be checked within the closure approximations.

As a final remark, we note that a modification of this model in order to take into account the non-zero correlation between velocity and magnetic field can be made (see the Appendix) by the use of a third parameter. This modification relies on the assumption that two different power laws exist for the $E^{\pm}(k)$ spectra at large scale, corresponding to a less-efficient beating for one of these two fields because of less transfer to small scales. Thus, from a numerical standpoint, the large scales of the flow in that case must be particularly well resolved, for example as in Chasnov (1995), at the expense of a lower Reynolds number. A numerical verification of this latter model is thus outside the scope of this paper, which concentrates on sufficiently well-resolved turbulent flows as relevant to astrophysics.

2.3. Inverse versus direct cascades as a criterion for decay laws

The phenomenological model developed here is independent of space dimension, except through the dependence of s itself. On the other hand, for incompressible neutral fluids, the 2D case is vastly different from the 3D case because of the lack of vortex stretching in two dimensions. This has led several authors, following Batchelor (1969), to consider the decay law of enstrophy $\Omega(t) = \langle \boldsymbol{\omega}^2 \rangle(t)$, where $\boldsymbol{\omega} = \boldsymbol{\nabla} \times \mathbf{v}$ is the vorticity. Assuming $\Omega(t) \sim (t-t*)^{-\zeta}$, a similar phenomenological analysis leads to $\zeta = 2$, for all s. This law was derived by Batchelor (1969) using the fact that energy undergoes an inverse cascade in 2D (see Fyfe and Montgomery (1976) and Fyfe et al. (1977); and Kraichnan and Montgomery (1980) for a review of 2D neutral and MHD turbulence). However, in MHD, there is no such constraint on energy, which cascades to small scales irrespective of the space dimension. To extend the phenomenology of Batchelor to MHD, one can nevertheless rely on the invariance of squared magnetic potential for $D = 2$ (Hatori 1984) and of magnetic helicity for $D = 3$ (Biskamp 1994). This approach, based on the existence of two invariants, leads for the decay of energy to a $(t-t_*)^{-1}$ law in 2D and to a $(t-t_*)^{-2/3}$ law in 3D. In the two-invariant model, the Reynolds number is then found to be constant in 2D and

increasing as $(t-t_*)^{1/3}$ in 3D, whereas it is constant for $s=1$ and always decreases for $s>1$ in the model proposed here, whatever the space dimension.

Numerical simulations in 2D with initial conditions centred on the large scales using periodic boundary conditions and with an initial correlation coefficient $\rho_0=\rho_C(t=0)\approx 10\,\%$, where

$$\rho_C=\frac{2\langle \mathbf{v}\cdot\mathbf{b}\rangle}{\langle |\mathbf{v}|^2+|\mathbf{b}|^2\rangle}, \tag{10}$$

indicate a $E_T(t)\sim(t-t_*)^{-1}$ behaviour, which can be interpreted through the constraint of the inverse transfer of the magnetic potential to large scales (Biskamp 1994). A different interpretation can be made in the context of the model proposed here with $s\to\infty$, i.e. corresponding to a constant integral scale, which also gives $E_T(t)\sim(t-t_*)^{-1}$. For $D=2$, we checked that a similar temporal dependence obtains at moderate resolutions using as initial conditions either the Orszag–Tang vortex, for which $\rho_0=50\,\%$, or random fields with $\rho_0\approx 10\,\%$; for both, inverse transfer is negligible, since $k_0\approx 1.5$ at $t=0$. In both sets of computations, error bars are large and one cannot ascertain which model is actually verified. However, the two-invariant model and the model presented here differ substantially in 3D. Numerical simulations on a uniform grid of 180^3 points indicate a *decrease* in the Reynolds number (Politano et al. 1995), although such computations clearly should be run for longer times and at higher Reynolds numbers, using for example an implementation of symmetries as in Brachet (1990) or a decimation algorithm as in Meneguzzi et al. (1996).

3. One-dimensional MHD

The phenomenology presented in this paper deals with the incompressible case, which is somewhat unrealistic as far as astro- and geophysical flows are concerned. The purpose of this section is therefore to explore the effect of compressibility in the simplest possible case, namely the one-dimensional case. In fact, the preceding phenomenology may apply as well to the 1D case with modifications that take into account the formation of shocks in the supersonic regime. This can be tested with high-resolution numerical simulations. Again, we shall be able to contrast the neutral case to the case of conducting fluids.

Indeed, when only derivatives in one space dimension are retained, one can no longer assume (except for the trivial case of constant fields) that $\boldsymbol{\nabla}\cdot\mathbf{v}=0$. The sets of equations must now include mass conservation. Computations with this slab geometry in MHD and with the assumption of a barotropic fluid (Gammie and Ostriker 1996) show that the decay is slower than for fluid turbulence.

In order to reach substantially higher resolutions, it is useful to consider, as a model, a cold plasma for which the pressure gradients are negligible, and the density is assumed constant. In that case, the 1D MHD equations reduce to:

$$D_t u=-\partial_x[\tfrac{1}{2}(b^2+c^2)]+\nu\partial_{xx}^2 u, \tag{11a}$$

$$D_t v=B_0\,\partial_x b+\nu\partial_{xx}^2 v, \tag{11b}$$

$$D_t w=B_0\,\partial_x c+\nu\partial_{xx}^2 w, \tag{11c}$$

$$D_t b=-b\partial_x u+B_0\,\partial_x v+\eta\partial_{xx}^2 b, \tag{11d}$$

$$D_t c=-c\partial_x u+B_0\,\partial_x w+\eta\partial_{xx}^2 c, \tag{11e}$$

with $D_t = \partial_t + u\partial_x$, the 1D Lagrangian derivative. The components of the velocity field are $\mathbf{v} = (u, v, w)$ and those of the magnetic field are $\mathbf{B} = (B_0, b, c)$. In the 1D case, the longitudinal component of the magnetic field, B_0, is constant since $\boldsymbol{\nabla}\cdot\mathbf{B} = 0$. For $B_0 = 0$, the dynamics of the two transverse components of the magnetic field is unchanged by the presence or absence of transverse components of the velocity, which thus play no particular role since they do not influence the dynamics of the longitudinal component of the velocity, and furthermore are simply advected. Thus, taking $B_0 = 0$ and $v = w = 0$, and introducing the change of variables $y^{\pm} = u \pm b$, the above equations can be written as

$$(\partial_t + y^{\pm}\partial_x)\, y^{\pm} = -\partial_x(\tfrac{1}{2}c^2), \tag{12a}$$

$$\partial_t c = -\partial_x[\tfrac{1}{2}(y^{+} + y^{-})\, c], \tag{12b}$$

omitting the dissipative terms for simplicity. With $c = 0$, the system (12) was introduced by Thomas (1968, 1970), and reduces to two Burgers equations for $y^{\pm}$. The energy decay of the Burgers equation is well known; in the standard case of initial conditions with, in the large scales, a spectrum $\sim k^s$, $s \geqslant 2$, one expects $E_{\mathrm{Burg}}(t) \sim t^{-1}$ (Kida 1979).

This value can be recovered phenomenologically on writing, in the presence of shocks, the large-scale spectra $\sim k^s$ with $s = D-1$ instead of $s = D+1$. Note that, contrasting the incompressible and compressible cases, this difference in large-scale spectral indices leads to a more important reservoir of energy at large scales for compressible flows when considering the effect of beating of two small-scale modes. These large-scale modes receive energy in equipartition, namely $E(k) \sim k^{D-1}$, whereas in the incompressible case the condition $\mathbf{k}\cdot\hat{\mathbf{v}}(\mathbf{k}) = 0$ implies symmetries of the second-order velocity correlation tensor, leading to a steeper energy spectrum $\sim k^{D+1}$, because of kinematic constraints as $\mathbf{k} \to 0$ (see, however, Saffman 1967a, b). Thus a smaller reservoir of energy obtains at large scales in the incompressible case, resulting in a faster decay; this is in contradiction with what is often expected when considering isolated shocks. The fact that an initially supersonic turbulent flow contains a large number of shocks has important dynamical consequences: these shocks, because of the presence of other shocks, are not always as steep as the viscosity would dictate for an isolated structure (Galtier 1998). Their interactions lead to the growth of the integral scale – an essential feature of turbulent flows, incompressible and compressible as well.

Furthermore, for a shock, the transfer time to small scales is independent of scale l (in that sense, the shock is a coherent structure, see e.g. Léorat et al. 1990). This time is proportional to $l_0/\Delta u_{\max}$, where l_0 is as usual the integral scale and $\Delta u_{\max}$ is the highest velocity jump, corresponding to the shock that forms first. Then

$$\alpha_{\mathrm{Burg}} = (s+1)\beta_{\mathrm{Burg}} = D\beta_{\mathrm{Burg}},$$

$$\epsilon_{\mathrm{Burg}}(t) \sim t^{-(\alpha_{\mathrm{Burg}}+\beta_{\mathrm{Burg}})} \sim t^{-(\alpha_{\mathrm{Burg}}+1)};$$

hence

$$\beta_{\mathrm{Burg}} = \alpha_{\mathrm{Burg}} = 1$$

for the 1D case treated here, corroborating the result of Kida (1979) for the energy.

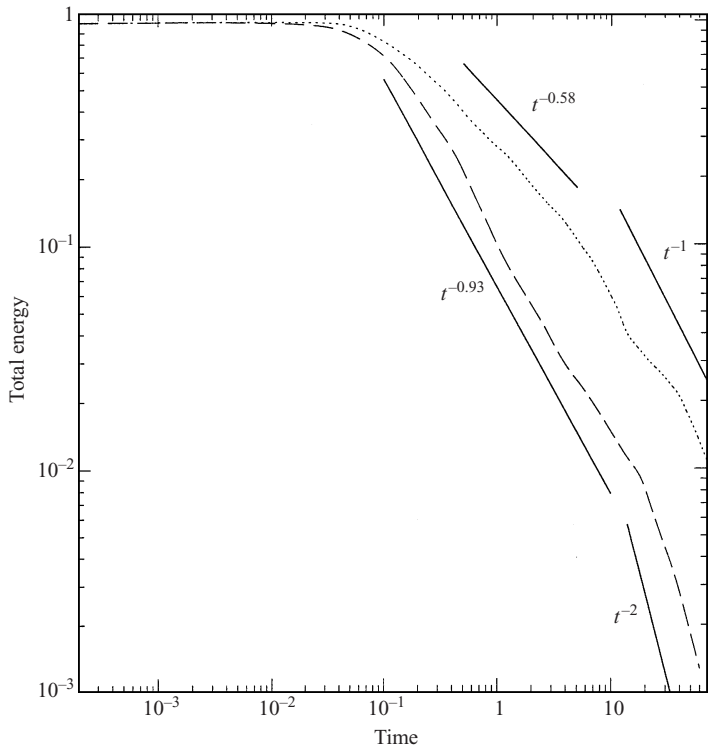

Figure 1. Temporal decay in log–log coordinates of the total energy in one dimension for the case of the Burgers-like equation (dashed line) and the MHD system (12) (dotted line). Note in both cases the emergence of a steeper time dependence at longer times, after the shocks have coalesced.

The introduction of a transverse component, $c \neq 0$, changes the problem altogether. Indeed, the equation (11e) for c is of the dynamo type: velocity gradients enhance the magnetic component in a time of the order of the turnover time (including in the absence of external forcing), and thus will affect directly the dynamics and the ensuing decay of energy, which also occur typically in a few eddy turnover times. The IK phenomenology may again apply, as long as the fluid is strongly compressible, $s = D-1$. For $g = 4$, one obtains $\alpha+\beta = 1$ with $\beta(D+1) = 1$, or, for $D = 1$,

$$\alpha = \beta = \tfrac{1}{2}.$$

At late times, however, there are no more strong shocks. Once all structures have merged, the integral scale becomes constant and the temporal decay law of the energy changes, with

$$(g-2)\,\alpha_{\mathrm{Burg}}^{(t^{\mathrm{sup}})} = 2,$$

irrespective of space dimension, since here β is assumed to be equal to zero. For $g = 3$, $\alpha_{\mathrm{Burg}}^{(t^{\mathrm{sup}})} = 2$ and for $g = 4$, $\alpha_{\mathrm{Burg}}^{(t^{\mathrm{sup}})} = 1$.

For a numerical integration of (12) on a grid of 8192 points, a power-law decay with $E(t) \sim (t-t_*)^{-0.64}$ was observed by Yanase (1997), with, under similar conditions, a $E(t) \sim (t-t_*)^{-1.15}$ behaviour for the Burgers case –

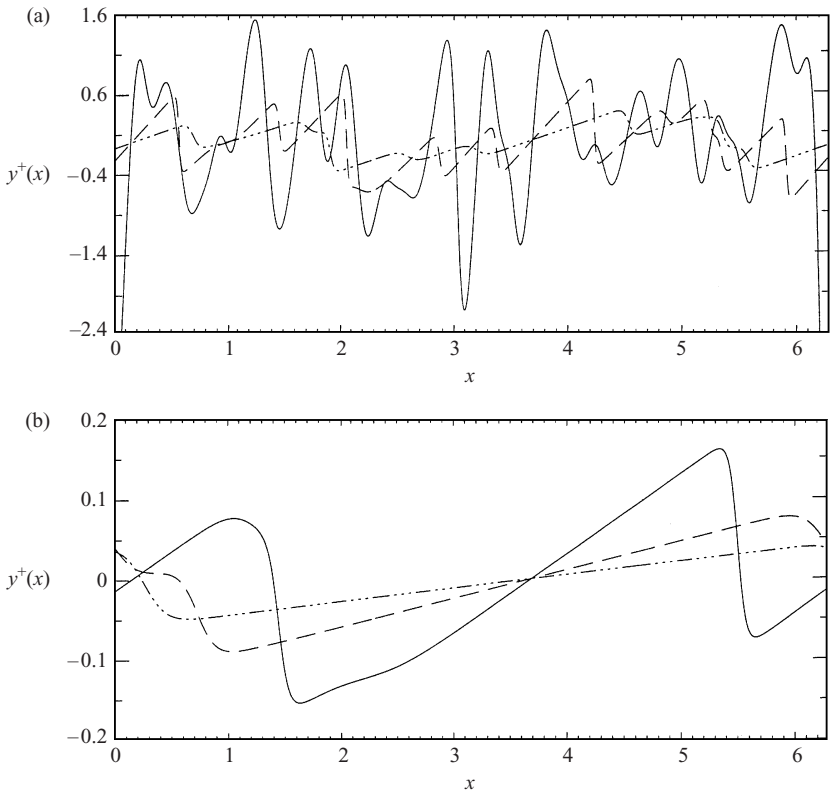

Figure 2. Coalescence of shocks for the one-dimensional Burgers run of Fig. 1 as viewed on the profiles of $y^+ = u+b$ at different times (see text). (a) displays times close to the maximum of $\langle(\partial y^+/\partial x)^2\rangle$, and (b) is for late times, corresponding to a different temporal regime once the integral scale cannot grow any further. Note the change of amplitude between (a) and (b).

somewhat steeper in both cases than the theoretically expected $(t-t_*)^{-1/2}$ and $(t-t_*)^{-1}$ decay laws. We have run a similar computation of (12) at the same resolution of 8192 grid points, but for longer times. We find that $E(t) \sim (t-t_*)^{-0.58}$ at intermediate times, whereas a similar run for the Burgers-like equation in terms of the $y^\pm$ variables produces a temporal evolution in good agreement with the linear decay law, namely $E(t) \sim (t-t_*)^{-0.93}$. Figure 1 displays in log–log coordinates this temporal evolution of the total energy for a Burgers (u, b) flow (dashed line) and for the helical MHD (u, b, c) flow (dotted line). Both sets show two different regimes in time; at later times, $E(t) \sim (t-t_*)^{-2.0}$ for the Burgers-like flow, and $E(t) \sim (t-t_*)^{-1.0}$ for the helical MHD flow – close enough again to the predictions of the model for late times.

In the framework of this 1D analysis, one can interpret the results by saying that magnetic fields prevent or slow down the formation of shocks and steep gradients: the motions have to work against the tension of magnetic field lines. This requires the presence of two transverse components of $\mathbf{b}$; otherwise, we recover the faster t^{-1} Burgers decay. When $c \neq 0$, the magnetic helicity $\langle \mathbf{a}\cdot\mathbf{b}\rangle$ (with $\mathbf{b} = \boldsymbol{\nabla}\times\mathbf{a}$) is non-zero. Its invariance in the non-dissipative case represents a topological constraint that helps preserve magnetic energy as well in the large scales, thus counterbalancing the effect of small-scale dissipative structures.

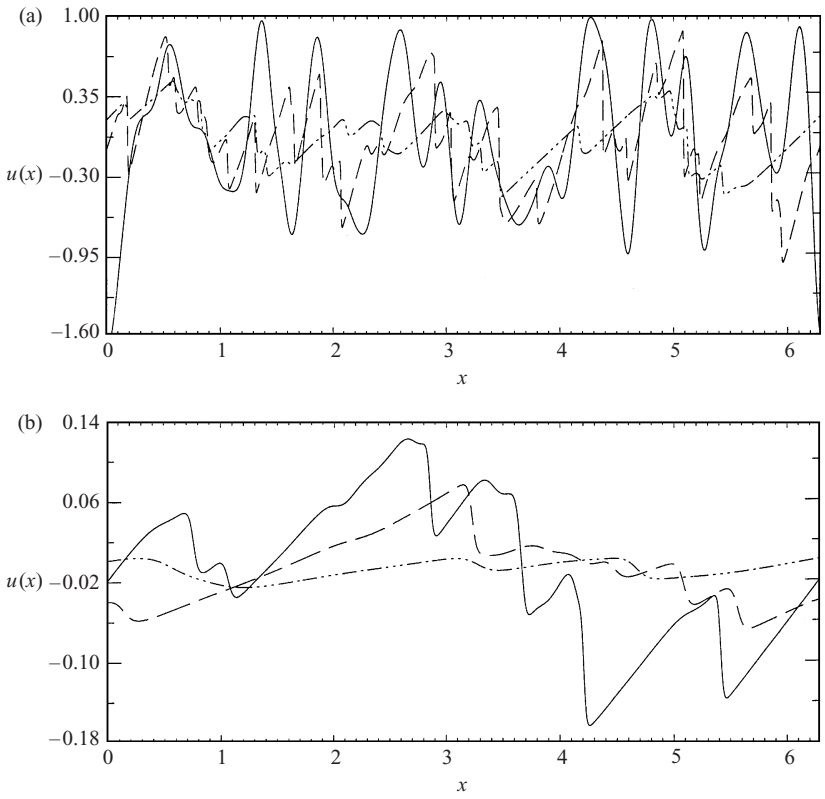

Figure 3. Coalescence of shocks for the one-dimensional MHD run of Fig. 1 as viewed on the profiles of the velocity u at different times (see text). (a) displays times close to the maximum of $\langle(\partial y^+/\partial x)^2\rangle$, and (b) is for late times.

The different regimes for intermediate times and for late times are linked to both

(i) the weakening of shocks, with, at late times, a moderately compressible flow as measured for example by the velocity jump in a typical structure;
(ii) the merging of shocks that have coalesced progressively – a signature (in terms of structures) of the growth of the integral scale.

This coalescence and weakening of shocks is visible in Fig. 2, which displays the $y^+ = u+b$ field for the Burgers-like equation, and in Fig. 3, which gives the velocity field for the helical MHD case of (12). In Fig. 2(a), the solid line corresponds to $t = 0.01$ (close to the time t_* of maximum enstrophy for that problem), the dashed line to $t = 0.6$ and the dash–dotted line to $t = 2$, whereas in the lower panel, the three times are $t = 10$ (solid line), 28 (dashed) and 60 (three dots–dashed). Note the change of scale by a factor of 8 for the amplitudes between the two panels. Similarly, in Fig. 3 (with solid, dashed and three dots–dashed lines as time increases), the times are 0.005 (again close to t_* for that problem), 0.05 and 1 for (a), and 7, 20 and 70 for (b), which again displays a substantially lower amplitude. When fronts have coalesced, as visible here in Figs 2(b) and 3(b), the growth of the integral scale is slowed down and a more efficient decay takes place.

This clearly confirms the important role in the law of energy decay of the dynamics of the characteristic scale of structures. It also provides a first approach to the understanding of the decay of compressible MHD flows, as already documented in the numerical simulations of Gammie and Ostriker (1996). In particular, shocks may be transient features of a non-universal nature for decaying turbulence – neutral or MHD – which obviously ends up being subsonic.

4. Numerical simulations in two dimensions

The model presented in this paper predicts in three dimensions for the standard MHD case ($g = 4$) a decay law $\sim (t-t_*)^{-5/6}$, very close to the prediction $(t-t_*)^{-1}$ of Hossain et al. (1995) based on a slightly different approach in which the Kolmogorov transfer time is retained. Several 3D numerical simulations (Hossain et al. 1995; Politano et al. 1995) indicate that the evolution of these runs is compatible with both laws, the data being insufficiently resolved to distinguish between the two models.

Resort to a simpler geometry has already been used in the past in order to be able to study MHD turbulence at high Reynolds numbers, the earliest work dating back to Fyfe and Montgomery (1976) (see also Fyfe et al. 1977). We follow this approach, and now report on a new series of numerical simulations performed for two dimensional incompressible MHD flows with periodic boundary conditions (see Stribling et al. (1994) for a discussion concerning the neglecting of the displacement current in that framework). Random initial conditions are taken for the $\mathbf{z}^{\pm}$ fields centred on $k_I = (s/2a)^{1/2} = 10$ with initial spectra proportional to $k^s e^{-ak^2}$. The parameters to be considered are the initial ratio of magnetic to kinetic energy $\chi = E^M/E^V$ (with $E^M = \frac{1}{2}\langle \mathbf{b}^2 \rangle$), the correlation coefficient between the velocity and magnetic field ρ_C, the presence or not of a uniform magnetic field B_0, and, from a numerical point of view, the algorithm used for dissipation (see below). Resolutions are from 512^2 up to 2048^2 uniformly spaced grid points. All runs are computed for about $10t_*$, where t_* is the time of the maximum of the total enstrophy $\langle |\boldsymbol{\omega}|^2 + |\mathbf{j}|^2 \rangle$, with $\mathbf{j} = \boldsymbol{\nabla} \times \mathbf{b}$ the magnetic current density. Table 1 gives a succinct description of the 2D runs presented in this paper.

The codes use a pseudospectral algorithm with a third-order Runge–Kutta time discretization for the nonlinear terms and a Crank–Nicolson time discretization for the linear terms. These codes are based on the magnetic potential and stream function variables. The dissipative terms are either standard Laplacians, which in Fourier space are $\nu k^2 \hat{\mathbf{u}}(\mathbf{k})$ and $\eta k^2 \hat{\mathbf{b}}(\mathbf{k})$, or they are modelled by a hyperviscosity algorithm whereby the above expressions are replaced by $\nu'_\gamma k^{2\gamma} \hat{\mathbf{u}}(\mathbf{k})$ and $\eta'_\gamma k^{2\gamma} \hat{\mathbf{b}}(\mathbf{k})$. In all cases, we take $\nu = \eta$ and $\nu'_\gamma = \eta'_\gamma$ as well, i.e. we choose a unit magnetic Prandtl number with identical powers of γ for the velocity and magnetic field of a given run.

The parallelized version of the code is based on the 2D fast Fourier transform (FFTs) provided by Cray for the T3E. The data format of the fields is adapted in such a way that the computational work is distributed over the allocated processors. A pseudospectral scheme is well suited for parallelization, because there is – except inside the FFTs – no time-consuming communication necessary between the processors, i.e. the computational work can be performed

Table 1. Nomenclature and main characteristics of the different two-dimensional runs presented in this paper.

Name	Run	N	γ	ν_γ	s	ρ_0	B_0	χ_0	α_N	β_N	
R24	1	512	1	2.0	3	0.04	0	1.1	1.06	0.42	*
R12	2	1024	1	1.5	3	0.04	0	1.5	0.95	0.32	
E1	3	2048	1	0.75	3	0.04	0	1.1	0.87	0.28	
E6	4	2048	1	0.19	3	0.04	0	1.1	0.77	0.39	
R23	5	512	2	1.0	3	0.04	0	1.1	0.70	0.34	*
R17	6	512	4	1.0	3	0.04	0	1.1	0.74	0.35	*
R22	7	512	8	1.0	3	0.04	0	1.1	0.77	0.32	*
R30	8	512	4	1.0	1	0.04	0	1.1	0.76	0.39	
R25	9	512	4	1.0	3	0.80	0	0.54	1.13	0.20	
E2	10	2048	1	0.75	3	0.80	0	0.65	1.21	0.33	
R26	11	512	4	1.0	3	0.04	1.1	1.1	1.06	0.00	
E3	12	2048	1	0.75	3	0.04	1.1	1.0	0.72	0.15	
R27	13	512	4	1.0	3	0.04	0	11.1	0.74	0.32	
E5	14	2048	1	0.75	3	0.04	0	11.3	0.77	0.40	
R28	15	512	4	1.0	3	0.04	0	0.11	1.08	0.35	
E4	16	2048	1	0.75	3	0.04	0	0.11	1.14	0.32	
R29	17	512	4	1.0	∞	0.04	0	0.3	0.71	0.37	

N is the one-dimensional resolution; γ is the index of the hyperdiffusivity coefficients ($\gamma = 1$ corresponds to the standard Laplacian); ν_γ is the viscosity or hyperviscosity coefficient in the dissipative terms, which are defined as $10^{n(\gamma)}\nu_\gamma$ for the corresponding values of γ and with enhancing factors of $n(1) = -3$, $n(2) = -7$, $n(4) = -16$ and $n(8) = -34$; s is the initial spectral index of the $E^{\pm}(k)$ spectra in the large scales; $\rho_0 = \rho_C(t = 0)$ is the initial correlation coefficient between the velocity and the magnetic field; B_0 is the amplitude of the uniform magnetic field; $\chi_0 = \chi(t = 0)$ is the initial ratio of magnetic to kinetic fluctuating energies. α_N and β_N are the exponents evaluated numerically on a time interval $[t_*, t_f]$. The exponents given here are in fact the means of the two $\pm$ exponents computed for the $\pm$ energy and integral scale. These two sets differ only by a few percent in all cases, except for runs 9 and 10, which are initially strongly correlated (see text). Runs marked with an asterisk have already been reported in Galtier et al. (1997).

locally on each processor on its own data. The parallelized code needs 4.8 s for one time step at the resolution 2048^2 with 32 processors on the T3E. This compares with 2.4 s computation time per time step for the vectorial code on the C90 (four processors) at the resolution 1024^2.

4.1. The decay law of the energy and integral scale

4.1.1. The standard case. We begin by reporting results obtained with the standard Laplacian diffusion operator, with $B_0 \equiv 0$, a negligible amount of correlation and $s = 3$ (Runs 1–4 in Table 1). The Reynolds numbers for these runs vary by a factor ten. The run with the lowest value (Run 1) has already been reported by Galtier et al. (1997).

The correlation coefficient $\rho_C(t)$ grows with time from 0.04 at $t = 0$ to 0.08 at the final time of the computation. Moreover, it remains small at all scales, as can be seen from inspection of Fig. 4 which displays for Run 4 the $E^{\pm}(k)$ spectra (respectively solid and dashed lines) at $t = t_* = 1.1$ (a). Indeed, the correlation $E^C = \langle \mathbf{v} \cdot \mathbf{b} \rangle$ is proportional to the difference between the two spectra, which is clearly negligible everywhere.

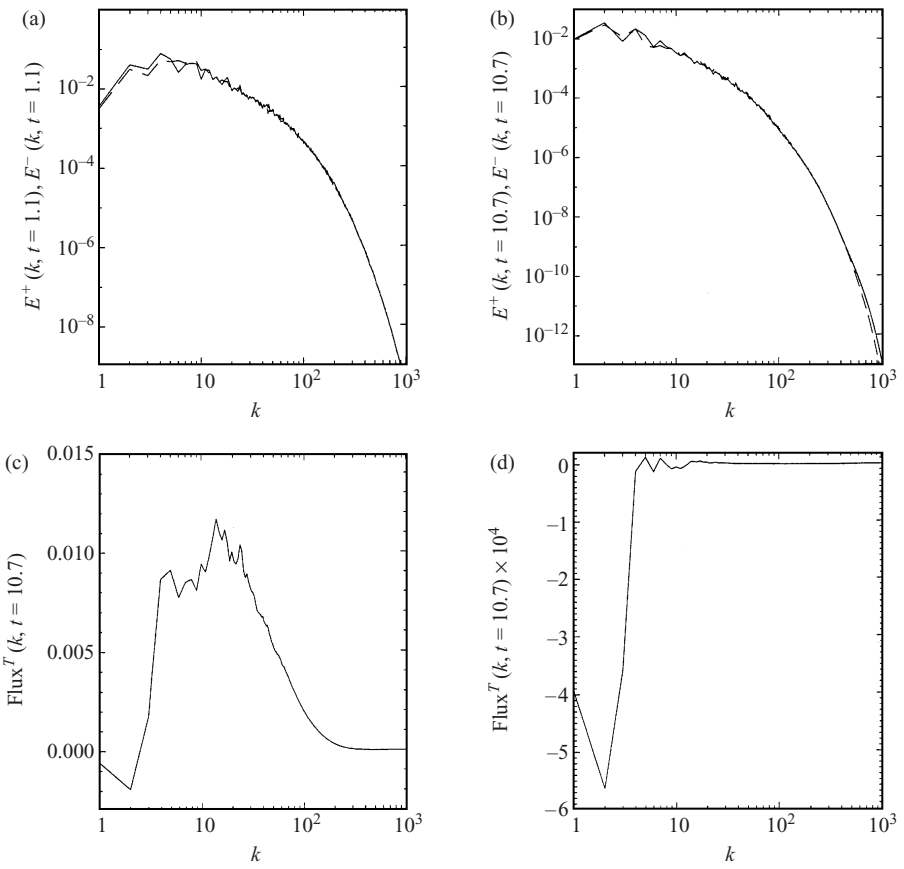

Figure 4. (a, b) $E^{\pm}(k)$ spectra for Run 4 at time of maximum enstrophy (a) and at the final time $t_f = 10.7$ of the computation (b). (c, d) Fluxes of energy (c) and of magnetic potential (d) at $t = t_f$. The width at half-maximum of the energy flux – where approximately constant – is a rough measure of the inertial domain, with here an extent from $k = 4$ to $k = 50$.

At the final time t_f of all runs (taken to be of the order of $10t_*$), only 10 % of the energy typically remains, and the ratio of magnetic to kinetic energy, initially close to unity, has grown by a factor of a little over two. Figure 4 also shows the $E^{\pm}(k)$ spectra at $t_f = 10.7$ for Run 4 (b), as well as, at the same time, the fluxes of the total energy (c) and of the magnetic potential (d). At this late time, the energy flux is still quasiconstant for a moderate span of wavenumbers, and the flux of magnetic potential is negative, corresponding to a small amount of inverse transfer of magnetic potential to large scales.

We give in Fig. 5(a) the temporal evolution of the total energy $E^T(t)$ in log–log coordinates for Runs 1–4 and Run 7 using a hyperdiffusive algorithm. A well-defined self-similar decay is visible on these curves, and is typical of all results reported in this paper. The equivalent temporal evolutions for the integral scale l_B for the same runs are given in Fig. 5(b) and the results of least-square fits to these laws, namely $E^T(t) \sim (t - t_*)^{-\alpha_N}$ and $l_B(t) \sim (t - t_*)^{\beta_N}$, are given in Table 1. The numerical exponents in Table 1 are the means of the + and − fields, with little variation between them except in the case of an initially strong correlation (see Sec. 4.1.5 for Runs 9 and 10). As the Reynolds number

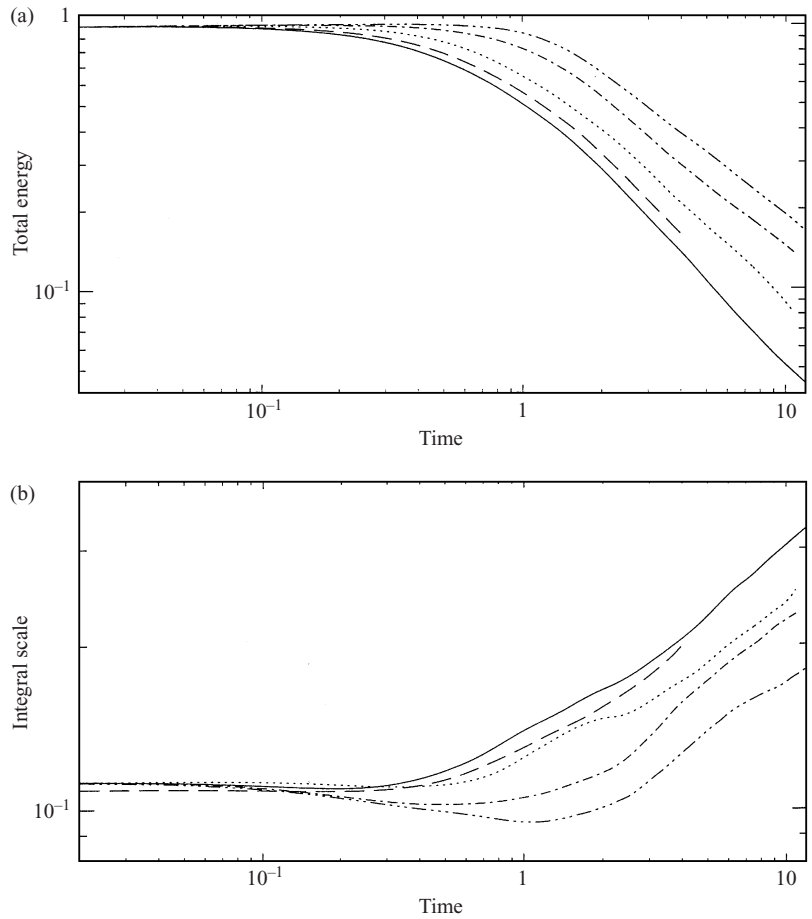

Figure 5. Temporal decay in log–log coordinates of the total energy (a) and the integral scale (b) for Run 1 (solid line), Run 2 (dashed), Run 3 (dotted), Run 4 (dot–dashed) and Run 7 (three dots–dashed). Note the delay in energy decay as the (effective) Reynolds number increases from Run 1 to Run 7 (see Table 1).

increases, a better separation obtains between the temporal decay due to a pure linear effect and that due to nonlinear interactions; at lower viscosity, the observed values are closer to the prediction of the standard model (here $\alpha_{4,3} = \frac{4}{5}$). Note also in Fig. 5 the delay in the onset of dissipation of energy as the Reynolds number R increases. This result is already known (Biskamp and Welter 1989; Politano et al. 1989; Passot et al. 1990), and is possibly linked to the 2D geometry, corresponding to an absence of singularity as $R \to \infty$ at early times, before reconnection takes place. In Fig. 6 are given the temporal evolution for Run 4 of the total (solid line), kinetic (dot–dashed) and magnetic (three dots–dashed) energies as well as the squared magnetic potential (dashed). Similar evolutions are observed for all computations.

4.1.2. The integral scale. Whereas for the energy, the discrepancy between the numerical values and the values of exponents predicted by the standard model is rather small at high Reynolds number, such is not the case for the integral scale, even though Fig. 5(b) shows that a power-law fit can be obtained. But the

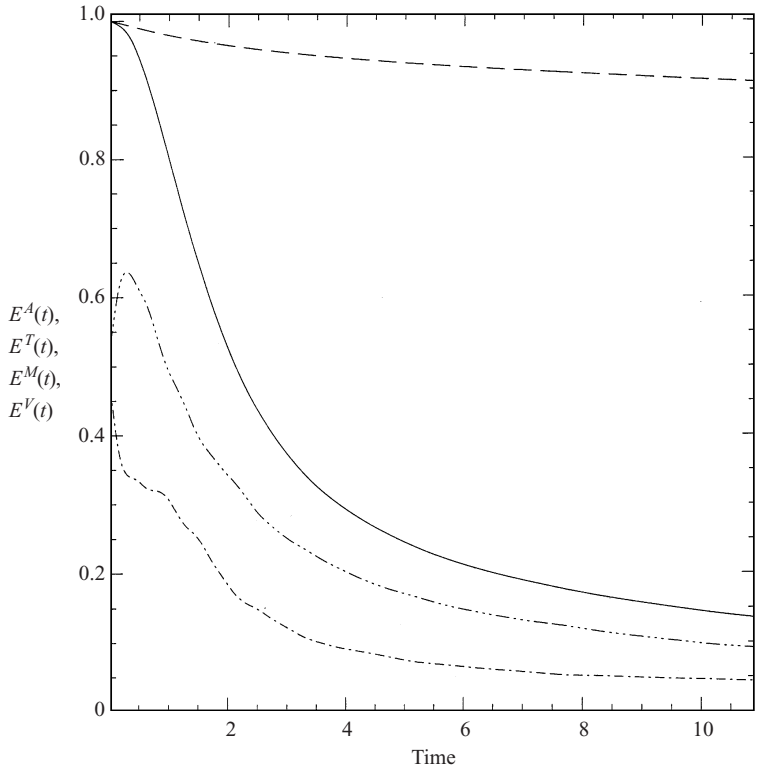

Figure 6. Temporal evolution for Run 4 of the squared magnetic potential (dashed line) and of the total (solid), kinetic (dot–dashed) and magnetic (three dots–dashed) energies.

slope does not correspond to the value predicted by our model with $s = 3$ and $g = 4$; this may be due to the fact that the temporal nonlinear range and dissipation range are not yet sufficiently well separated. Moreover, it may be more difficult to model the evolution of l_B, because it is more sensitive than the energy to boundary effects close to $k = k_{\min}$, in particular because there is an inverse transfer of $\langle \mathbf{a}^2 \rangle$ (where $\mathbf{b} = \boldsymbol{\nabla} \times \mathbf{a}$) creating excitation at large scales. Here again, the numerical resolution is crucial in order to separate all such spatial and temporal intervals, so that no effect of one range be felt on the other one – otherwise computed values of exponents could be fudged by these boundary effects. With $k_I = 10$, the scale separation may be insufficient.

4.1.3. The hyperdiffusive case. The temporal evolutions for Runs 5–7 using a hyperdiffusive algorithm have already been reported in Galtier et al. (1997) (see fig. 1 of that paper). For such hyperviscous runs, the squared magnetic potential changes very little with time (for example, in Run 6, by less than 0.1%), the dissipation being strongly concentrated in the small scales and negligible in the large scales.

The results on temporal decay laws show that hyperdiffusive algorithms do not lead to substantially different scaling exponents when compared with the standard case using a Laplacian operator (see, however, Sec. 4.2 for the case of higher-order moments). It is known that for the passive scalar, analytical calculations of anomalous exponents of structure functions show a lack of

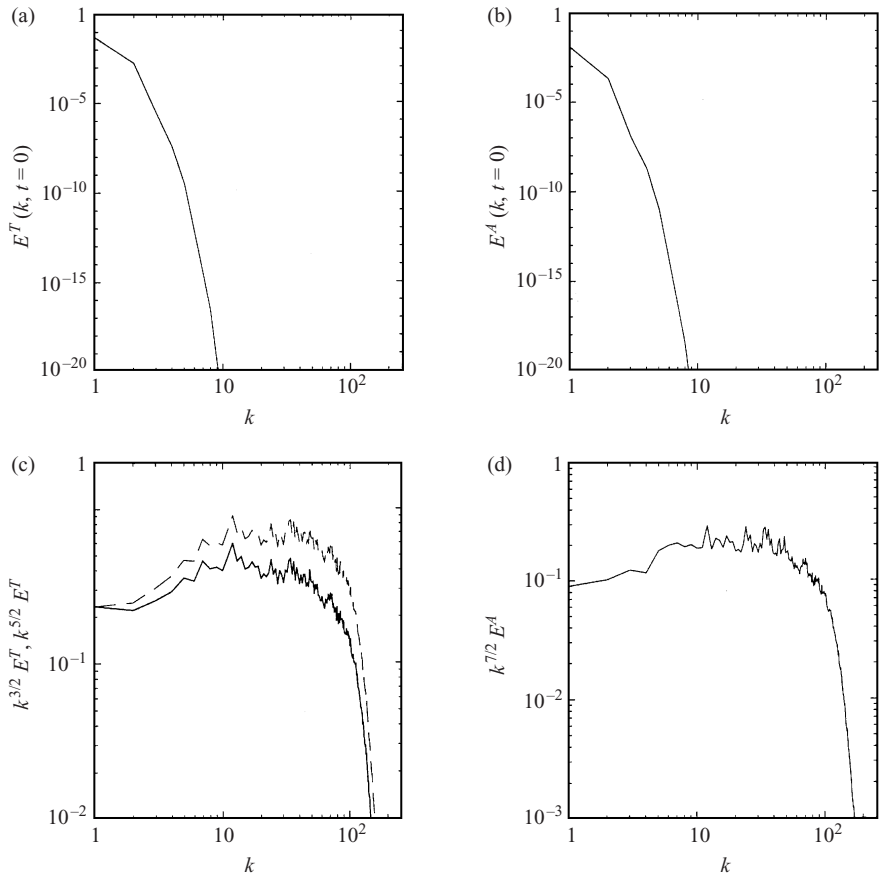

Figure 7. Spectra for Run 17 in log–log coordinates of (a) the total energy $E^T(k)$ and (b) the magnetic potential $E^A(k)$ at $t = 0$. At $t = 10.7$, the following compensated spectra are shown: (c) $k^{3/2}E^T(k)$ (solid line) and $k^{5/3}E^T(k)$ (dashed); (d) $k^{7/2}E^A(k)$. Note that both the IK and K41 spectral laws would be acceptable. The ambiguity stems from the fact that intermittency corrections steepen the IK law, as they are known to do for the K41 law.

sensitivity to the precise way in which the variance of the scalar is being dissipated in the specific framework of hyperviscosity models (Eyink 1996), simply because the turbulent diffusivity overwhelms the linear one. Therefore, in all of the subsequent parametric study, only two runs will be performed for each case, one on a grid of 2048^2 points with $\gamma = 1$ and one on a grid of 512^2 points with $\gamma = 4$ (see Table 1); however, for Runs 8 and 17 (with $s \neq 3$), only one type of run, with $\gamma = 4$, is performed.

4.1.4. The large-scale spectrum of energy. The hyperdiffusive algorithm is now used to study the role of the parameter s, i.e. of the spectral slope at large scales, on decay laws.

To that effect, we examine two simulations (Run 8 with $s = 1$ and Run 17 with $s \to \infty$). We show in Fig. 7 the spectra of total energy $E^T(k)$ (a, c) and magnetic potential $E^A(k)$ (b, d) at $t = 0$ (a, b) and $t = 10.7$ (c, d) for Run 17. At $t = 10.7$, the spectrum of magnetic potential is compensated by a $k^{7/2}$ law, whereas for the energy, two compensated spectra are shown: the solid line

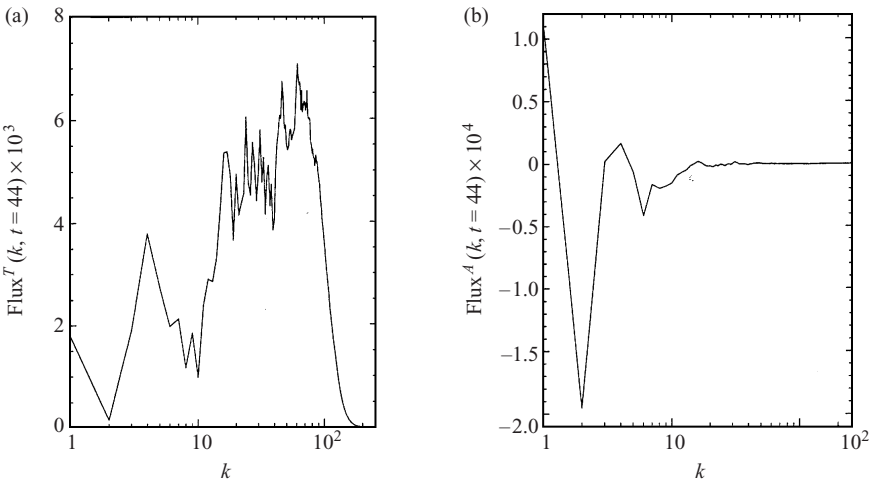

Figure 8. Spectra at $t = 44$ for Run 17 using hyperviscosity of the flux of energy (a) and the flux of magnetic potential (b). Note that the latter is negative, indicative of inverse transfer. The inertial range extends significantly closer to the cut-off wavenumber of the computation than with a standard Laplacian as used in the run of Fig. 4.

shows $k^{3/2}E^T(k)$ and the dashed line $k^{5/3}E^T(k)$. Differentiation between the IK and K41 spectral laws is difficult, in part because of the steepening of the first-order similarity scaling due to intermittency corrections (see the discussion of this point in Sec. 5).

In Fig. 8 the fluxes of energy (a) and of magnetic potential (b) are displayed at the final time $t_f = 44$. As for Run 4, there is a slight build-up of magnetic potential in the large scales over time. This can be related to the fluxes: whereas energy flows to small scales (positive flux, quasiconstant over a large range of wavenumbers – a phenomenon common to hyperdiffusive simulations), the magnetic potential flows to large scales, with a substantial flux that is negative for small wavenumbers.

Run 17 was done in an attempt to have a constant integral scale; in fact, this scale grows with time as shown in Fig. 9(b). Figure 9(a) displays the total E^T (solid line), kinetic E^V (dashed) and magnetic E^M (dotted) energies as functions of time. In this run using hyperviscosity, negligible energy dissipation occurs for $t < t_*$, and clear Alfvénic exchanges between E^V and E^M are observed up to t_*, the large-scale magnetic field playing the same role as a uniform magnetic field.

The measured exponents given in Table 1 for the decay laws for Runs 8 and 17 do not agree with the prediction of the model; rather, they are quite close to all other cases tested in this paper. The origin of this discrepancy is clear: it is not so much that the model fails, it is rather our inadequacy at controlling, as time evolves, the parameter s, i.e. the slope of the energy spectrum at large scales. This may be related, as stated before, to insufficient scale separation between k_I and $k_{\min}$. Other runs would have to be performed to check this point. In fact, another conclusion can be drawn: the standard model with $g = 4$ and $s = 3$ proves to be relevant in most cases because a k^{D+1} spectrum develops at large scales (through eddy noise) by nonlinear interactions. Thus the parameter s itself ends up not being an open parameter of the problem, but rather one that,

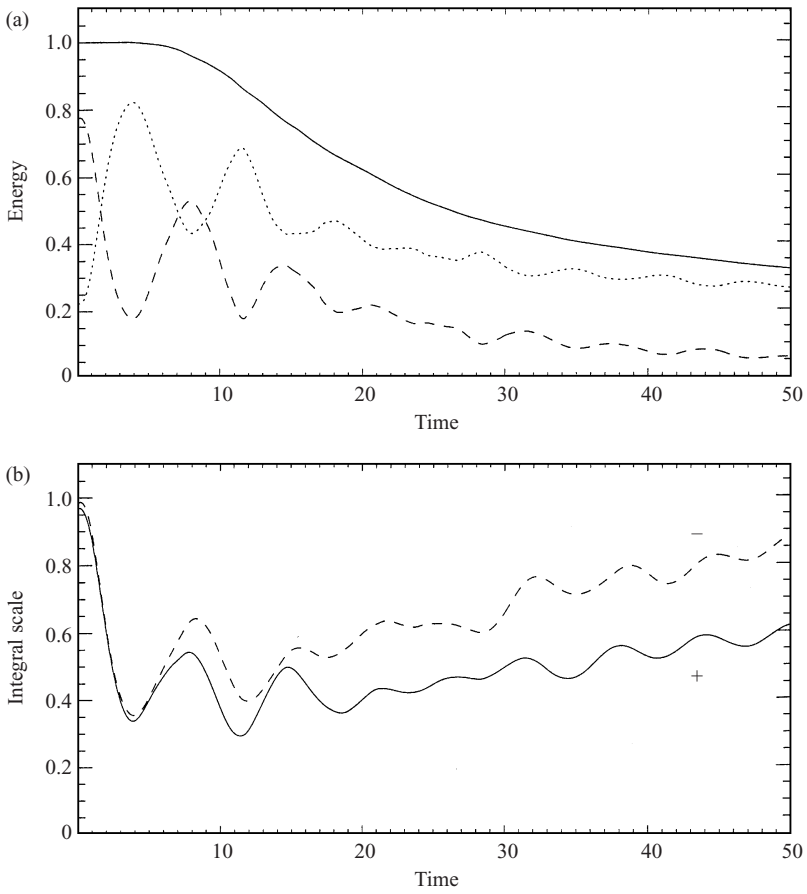

Figure 9. Temporal evolutions for Run 17 of the total (solid line), kinetic (dashed) and magnetic (dotted) energies (a), and of the $\pm$ integral scales (b). Note the almost-inviscid exchanges between kinetic and magnetic energies at early times.

in most cases (i.e. unless one controls the integral scale), is governed by the dynamics.

4.1.5. Velocity–magnetic-field correlation. In Runs 9 and 10, the velocity–magnetic-field correlation is strong initially ($\rho_0 = 0.80$). In this case, the nonlinear terms in the MHD equations cancel almost exactly at all points in space and the transfer of energy to small scales is considerably diminished. For example, at $t = 8$ (or $13\,t_*$), the remaining energy is 13 % of its initial value for Run 3, and 17 % for Run 4 to be contrasted with 38 % for run 10.

The temporal evolution of $E^{\pm}(t)$ for Runs 9 and 10 is shown in Fig. 10(a). The $E^{\pm}(t)$ energies (and the $\pm$ integral scales, which are not shown) evolve at different rates. For Run 10, we find $E^{+}(t) \sim (t-t_*)^{0.66}$ and $E^{-}(t) \sim (t-t_*)^{-1.75}$. This implies that the velocity–magnetic-field correlation, as expected, increases with time, since it is proportional to the difference $E^{+}(t)-E^{-}(t)$. For the integral scale, we find $l_B^{+}(t) \sim (t-t_*)^{0.23}$ and $l_B^{-}(t) \sim (t-t_*)^{0.42}$. The equivalent exponents for Run 9 are respectively 0.26, 2.0, 0.12 and 0.29. Again, both sets of runs with either a standard Laplacian at a resolution of 2048^2 grid points or with a

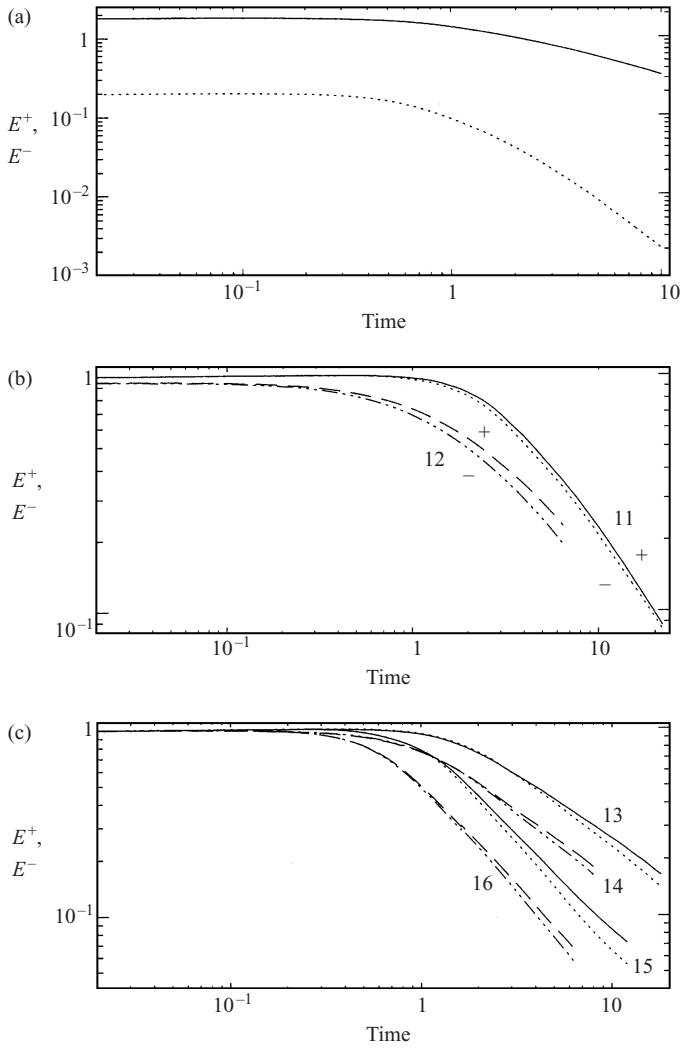

Figure 10. (a) Temporal decay of E^+ (solid line) and E^- (dotted) for Run 10 with initially a high correlation coefficient $\rho_0 = 80\,\%$. (b) $E^{\pm}(t)$ for Runs 11 and 12 in the presence of a strong uniform magnetic field $B_0 = 1.1$. (c) $E^{\pm}(t)$ for Runs 13–16 with an initial magnetic to kinetic energy ratio χ_0 differing from unity (see Table 1). All curves are in log–log coordinates, and in all cases the correlation is positive ($E^+ \geqslant E^-$); hence the curve corresponding to E^+ is systematically above that for E^-; no substantial difference in the decay rates of $E^{\pm}$ is seen.

hyperviscous algorithm with $\gamma = 4$ on a rid of 512^2 points give the same overall picture. We note that the *average* values of the exponents for the two fields fall not too far from those predicted by the present model. This is reminiscent of the different indices that obtain for the $\pm$ energy Fourier spectra in the strongly correlated case; it is shown in Grappin et al. (1983) that, with $E^{\pm}(k) \sim k^{-m_{\pm}}$ in the inertial range, a simple phenomenological argument gives $m^+ + m^- = 3$, a law compatible with the standard IK spectral indices, namely $m^+ = m^- = \frac{3}{2}$, corresponding to the uncorrelated case with identical $\pm$ scaling. Such results were confirmed by computations performed both with second-order closures

(Grappin et al. 1983) and with 2D numerical simulations (Politano et al. 1989). In Fig. 10, we also show the temporal evolution of $E^{\pm}$ for Runs 11 and 12 (b) and Runs 13–16 (c); all curves are labelled by the number of the run, the + energy being systematically slightly above its negative counterpart. Note that there is no noticeable variation in the rates of energy decay when contrasting the + and − fields.

4.1.6. Is the decay modified in the presence of a uniform magnetic field? A uniform magnetic field is an important feature of many realistic MHD flows, in the laboratory (such as in tokamaks) as well as in astrophysical plasma such as the solar wind and the interstellar medium. The presence of B_0 is known to lead to the development of anisotropies, the energy transfer being strongly inhibited for wavenumbers parallel to the uniform field (Shebalin et al. 1983; Oughton et al. 1994). Furthermore, when B_0 is strong enough that neutral X points are absent, it impedes the development of small scales altogether, as measured for example from the temporal evolution of the logarithmic decrement of the energy spectrum (Frisch et al. 1983). This latter fact leads to a choice for the amplitude of B_0 such that the resulting total magnetic field has no neutral X points. We also explicitly checked that there are neutral X points in the runs with $B_0 \equiv 0$. For Runs 11 and 12, $B_0 = 1.1$, to be compared with the r.m.s. values of the velocity and magnetic field equal to unity; this choice of B_0 for the computations to be reported now allows one to keep an explicit temporal scheme. The temporal scaling laws with $B_0 \neq 0$ can be examined by inspection of the data given in Table 1, for Runs 11 and 12. No substantial effect is to be discerned, at least at this amplitude of B_0, which is comparable to the r.m.s. values of the fluctuating fields – as is observed in the interstellar medium (Heiles et al. 1993). This confirms that the IK phenomenology works in the same way for a mean magnetic field or for its large-scale component, provided that there is a sufficient scale separation in the dynamics of the turbulent magnetic field, with a large range of excited scales.

4.1.7. Initial ratio of kinetic to magnetic energy. The last parameter that we consider is linked with selective decay. It was shown by Matthaeus and Montgomery (1980) (see also Matthaeus and Montgomery 1984; Ting et al. 1986) that for an initial ratio of magnetic to kinetic energy $\chi = E^M/E^V$ significantly different from unity, different regimes may occur, namely a hydrodynamical regime when $\chi \ll 1$, a magnetic regime when $\chi \gg 1$ and the correlated regime when initially $\chi \approx 1$. Here we tested the effect that χ may have on energy decay laws by varying this parameter in a range of 100 (Runs 13–16). The resulting temporal decay laws are given in Table 1. The values again do not differ substantially from those found previously. We note here that for most runs of Table 1, χ evolves over time to values close to 2, including for Runs 13–16. However, it is substantially closer to unity for the runs with either a strong B_0 or a strong correlation coefficient, as shown in Fig. 11 for Run 4 (solid line), Run 12 (dashed), Run 14 (dot–dashed) and Run 16 (dotted). Run 12 displays more-regular fluctuations, with a period of oscillation $2\pi/(k_I B_0)$ corresponding to the Alfvén time constructed on the energy-containing wavenumber k_I. Note also the slight excess of magnetic energy in all cases, as often observed in the solar wind (Matthaeus and Goldstein 1982).

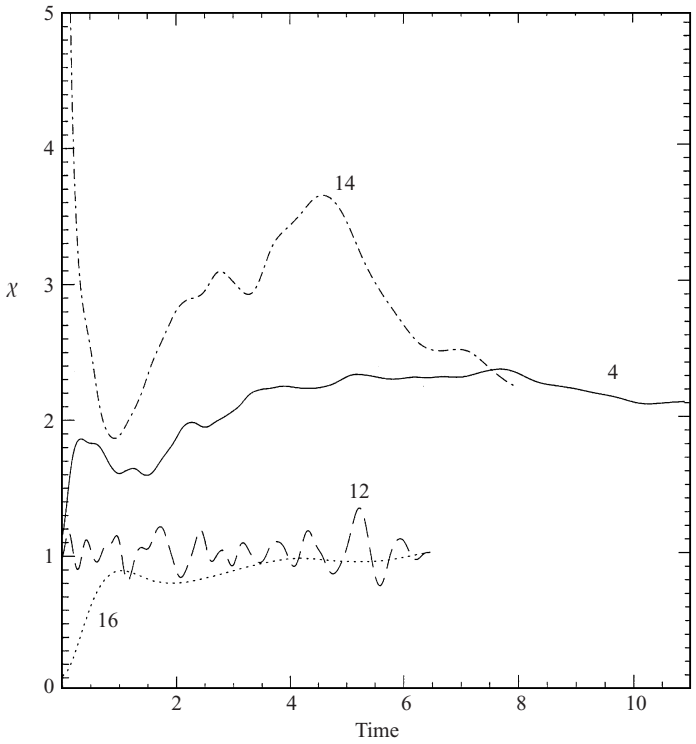

Figure 11. Temporal evolution of the ratio $\chi = E^M/E^V$ for Runs 4 and 12 (both with $\chi_0 = 1$), Run 14 ($\chi_0 = 10$) and Run 16 ($\chi_0 = 0.1$) (see Table 1); curves are labelled with the run number. The oscillations for Run 12 are due to the presence of a uniform component of the magnetic field for that run. In all cases, equipartition obtains with a slight excess of magnetic energy, as is also observed in the solar wind.

We thus conclude that the initial value of χ, unless drastically different from unity, may again be an irrelevant parameter because χ evolves rapidly in the initial phase, before t_*, to a value close to unity.

4.2. Temporal evolution of higher-order moments

The phenomenological model presented in Sec. 2 can be extended to predict the temporal decay of higher moments of the Elsässer fields, by simple dimensional analysis using the temporal variation of the two fundamental variables $z^\pm \sim z$ and $l^\pm \sim l_B$. For example, assuming negligible velocity–magnetic-field correlations, the generalized $\pm$ palinstrophies $\mathscr{P}^\pm = \langle|\boldsymbol{\nabla}\times(\boldsymbol{\nabla}\times\mathbf{z}^\pm)|^2\rangle$ decay as $z^2 l_B^{-4}$, and thus

$$\mathscr{P}^\pm(t) \sim (t-t_*)^{-p_s}, \tag{13}$$

with

$$p_s = \frac{2(s+5)}{g(s+1)-2s}. \tag{14}$$

Similarly, one can compute the temporal evolution of the q-moments of the $\pm$ vortices $\boldsymbol{\omega}_\pm = \boldsymbol{\omega}\pm\mathbf{j}$, which scale as $(z/l_B)^q$. One find

$$\langle|\boldsymbol{\omega}\pm\mathbf{j}|^q\rangle(t) \sim (t-t_*)^{-\delta_{q,s}}, \tag{15}$$

with

$$\delta_{q,s} = \frac{s+3}{g(s+1)-2s} q, \tag{16}$$

whereas for neutral fluids ($\mathbf{j} \equiv 0$) in 2D, one has $\delta_{q,s} = q$ independently of the value of s, following the Batchelor phenomenology (Bartello and Warn 1996). Numerically, for Run 7 with $\gamma = 8$ and $s = 3$, we find $p_3 = 1.20 \pm 0.03$, to be compared with the theoretical prediction of $\frac{8}{5}$ for $g = 4$. Similarly, one has $\delta_{2,3} = \frac{6}{5}$ for $q = 2$ and $g = 4$, to be compared with $\delta_{2,3} = 1.09 \pm 0.02$ for the present computations; note that in Kinney et al. (1995), one finds $\delta_{2,3} = 1.30 \pm 0.04$.

We have evaluated $\delta_{q,3} = F^{\pm}(q)$ for the $\pm$ fields for Runs 3, 4 and 7 (all with $s = 3$) for $q = -\frac{1}{3}, +\frac{1}{3}, \frac{2}{3}, 1, \frac{3}{2}, 2, 3, 4, 6, 8$ and 10. Writing

$$F^{\pm}(q) = -a^{\pm} q, \tag{17}$$

the prediction of (16) with $g = 4$ gives $a^{\pm} = \frac{3}{5}$, whereas for Run 4, we find values of 0.73 and 0.84 for the $\pm$ fields respectively. The top row of Fig. 12 gives $F^{+}(q)$ for Run 4(a), Run 3(b) and Run 7(c). On breaking this law into separate dependences for the q-moments of the current (d–f) and the vorticity (g–i), similar linear laws obtain for the current, whereas the vorticity shows, for $q \geqslant 4$, a much shallower variation with q, with a slope equal to 0.08, a result reminiscent of the Navier–Stokes case (Bartello and Warn 1996). Run 3 at a lower Reynolds number gives a linear dependence as well, but with a different coefficient, namely $a^{+} \approx 1.4$, a result attributable to the lack of development of that flow and with structures in insufficient numbers. Run 7 using hyperviscosity gives similar results at low q, with $a^{+} \approx 0.69$ up to $q = 2$, after which the relationship curves upward in a parabolic way. Finally, Figs 12(j–l) give in log–log coordinates the data versus time from which the slopes are computed. They display the increasing range of uncertainty, as q increases, in determining these slopes.

One can find wide variations in the literature concerning the values of the computed exponents of high order for the decay in two dimensional Navier–Stokes flows (Carnevale et al. 1991, 1992; Dritschel 1993; Bartello and Warn 1996; Chasnov 1997). The reasons for such variations are far from understood. It could be that there is no universality, and initial conditions (e.g. enstrophy-dominated versus energy-dominated flows), Reynolds numbers and boundary conditions may have to be taken into account; the numerical methods (pseudospectral codes with or without hyperviscosity, finite-difference codes, contour surgery) may alter the results as well. The data presented here indicate that, at the energy level, hyperviscous algorithms are adequate; but as one increases the order of the moments, putting more emphasis on the strong small-scale features, the results differ between a standard Laplacian and a hyperdiffusive algorithm for orders greater than two. This can be understood on realizing that such algorithms alter the dissipation, leading to distorted structures with ghosts. Figure 13 shows, at the final time of the computation, the contours of the current density for Runs 4 and 7. The formation of strong curved current sheets, and of large-scale and small-scaling dipoles, is clearly seen (see also Kinney et al. 1995), as is the more spotty aspect of these structures in the hyperdiffusive case. One can state that, on average, energy dissipation is adequately represented with such hyperdiffusive algorithms, because energy dissipates at a rate that is mostly set by the turbulent eddy

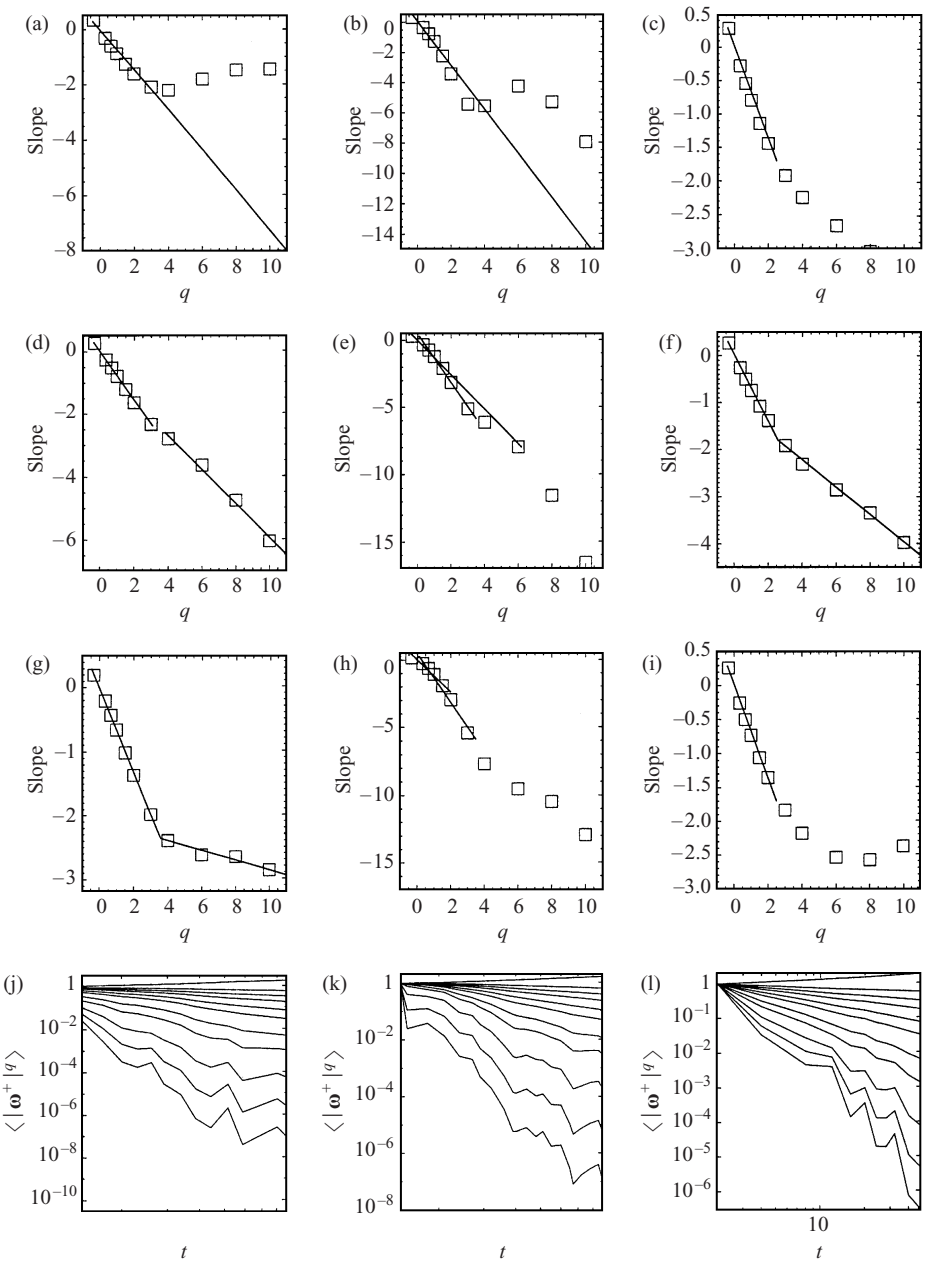

Figure 12. (a–c) Scaling behaviour of q-moments of the generalized vorticity $|\boldsymbol{\omega}^+|^q$ for Run 4 (a), Run 3 (b) and Run 7 (c). For the same runs, (d–f) show $|\mathbf{j}|^q$ and (g–i) show $|\boldsymbol{\omega}|^q$. (j–l) display in log–log coordinates the scaling dependence with time of $|\boldsymbol{\omega}^+|^q$, from which the slopes are computed. The order q varies from $q = -\frac{1}{3}$ to $q = 10$ (see text), increasing from bottom to top.

viscosity, which overwhelms the linear terms (see Eyink (1996) for a passive scalar); but coherent structures block transfer to some degree, and higher-order moments of the velocity and magnetic fields feel their effect more strongly, because they are more sensitive to their boundaries. Hence these algorithms

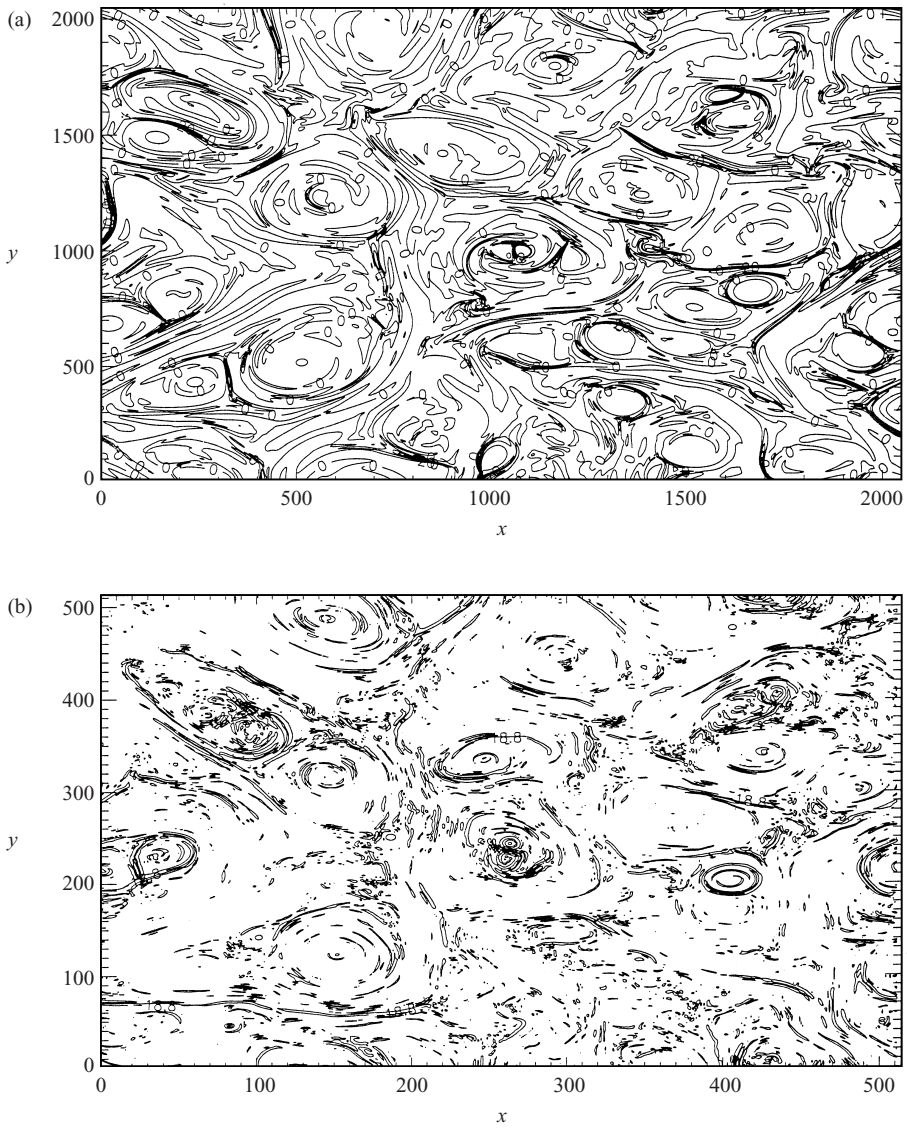

Figure 13. Contours of the current density at the final time of the computation, namely $t_f = 10.7$ for Run 4 (a) and $t_f = 12$ for Run 7 (b). Note the spatial self-similarity of the flow with embedded structures, which is particularly visible in the hyperviscous case of Run 7.

become less reliable when examining the behaviour of higher-order moments, because they do not reproduce accurately the inner spatial configuration of dissipative structures.

5. Discussion and conclusions

Following the Kolmogorov (K41) phenomenology for neutral fluids, we have derived for MHD a model of self-similar energy decay that relies on the persistence of large-scale eddies and on a phenomenological evaluation of energy transfer to small scales that takes into account the slowing-down of

nonlinear mode coupling as described in the Iroshnikov–Kraichnan (IK) phenomenology. A simple extension of the model allows for the prediction of the decay of higher moments of the velocity and magnetic fields (see Bartello and Warn (1996) for the fluid case). Intermittency effects might then have to be taken into account for high orders, using for example the p-models for MHD (Carbone 1993) or the She–Leveque (1994) model for MHD (Grauer et al. 1994; Politano and Pouquet 1995).

No experimental data are available at high magnetic Reynolds number, so that numerical simulations should be particularly useful in differentiating between the K41 and IK temporal behaviours (both in the solar wind and in the interstellar medium observational data do not give direct access to temporal decay). This differentiation is easier for the temporal decay laws, which differ substantially ($\frac{10}{7}$ for K41 versus $\frac{5}{6}$ for IK in three dimensions), than for the equivalent problem of distinction between the spectral indices for inertial ranges ($\frac{5}{3}$ for K41 versus $\frac{3}{2}$ for IK). Such a differentiation between K41 and IK temporal scaling may also be amenable to verification using either second-order closures or shell models of MHD turbulence, which in both cases allow for substantially higher Reynolds numbers, or using some kind of modelization, such as in sparse methods with a reduced set of wavenumbers (Grossman and Lohse 1991; Meneguzzi et al. 1996), or enforcing symmetries as in Brachet (1990) (for MHD, see Nore et al. 1997).

The differentiation between the IK and the K41 phenomenology is in fact the main underlying motivation for this work. Indeed, as noted above, this differentiation is difficult for Fourier spectra. And this is all the more so when one takes into consideration the corrections stemming from intermittency (for a review, see Frisch 1995), which are known to render the spectra steeper in a direct energy cascade. Hence the K41 $\frac{5}{3}$ law for the energy spectrum $E(k)$ becomes, as experimentally measured and as predicted by a phenomenological model, $E(k) \sim k^{-1.70}$ (see She and Leveque 1991, and references therein). It should be noted that in the solar wind, Voyager data indicate that the inertial index of the energy spectrum is close to 1.66 (Matthaeus and Goldstein 1982). This can of course be interpreted as a K41 spectrum, i.e. neutral incompressible fluid turbulence phenomenology would seem to apply in the context of the compressible plasma flow of the solar wind. On the other hand, such a flow is at a high Reynolds number, and hence intermittency corrections should be present. Therefore a different interpretation is that this spectrum is a trace of a strongly intermittent magnetized Alfvénic flow. Indeed, MHD flows are known to be more intermittent than neutral fluids, as characterized by the Batchelor analogy assimilating the magnetic induction to the vorticity field, and as found in numerical simulations (Politano et al. 1998; Galtier et al. 1998) and in the solar wind data analysed by Burlaga (1991), although the sample is of too moderate a size for firm conclusions to be reached (see also Dudok de Wit and Krasnosel'skihk 1996). However, as noted before, the difference in the decay laws for neutral fluids and conducting fluids is large enough that the IK and K41 laws can be differentiated with present-day data. Hence we can conclude from the temporal analysis presented in this paper that MHD flows probably follow an evolution encompassed by the IK model as opposed to pure advection.

The lack of dependence in (8) on the global correlation coefficient is assumed,

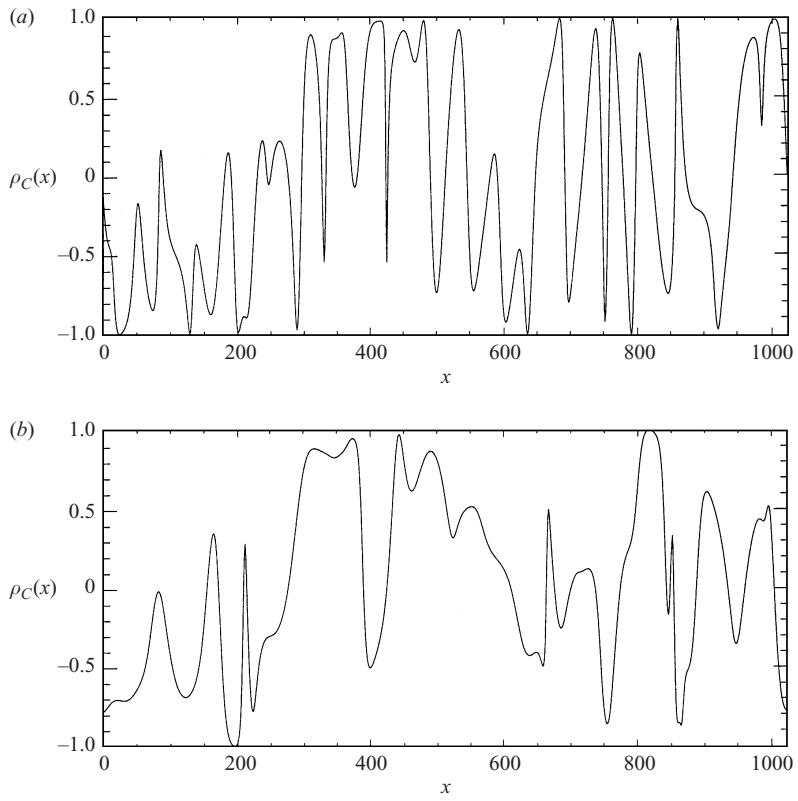

Figure 14. One-dimensional cut for Run 2 at $y = \pi$ of the pointwise correlation coefficient $\rho_C(\mathbf{x})$ at $t = 0$ (a) and at the final time of the computation $t_f = 4$ (b). Note the temporal growth in characteristic scale and the strong local values of ρ_C at both times, although the integrated correlation coefficient is weak.

but is not necessarily paradoxical if one recalls that the velocity–magnetic-field correlation is not positive-definite: even a moderate global value of ρ_C can hide high local values of opposite signs. It is known that correlations develop in time (Matthaeus and Montgomery 1980; Ting et al. 1986), and that the flow organizes in several bipolar sets of regions with strong $\pm$ values of the correlation coefficient, i.e. with correspondingly weak nonlinearities except at the borders of those regions where all small-scale activity takes place, in particular in the formation and disruption of current and vorticity sheets. Indeed, we show in Fig. 14 a one-dimensional cut of the local correlation coefficient $\rho_C(\mathbf{x})$ for Run 2 at $t = 0$ (a) and at the final time of the computation (b). Between the two times, one can note the increase in the characteristic scale of the flow. More importantly, although the global correlation in this run is weak ($< 5\,\%$ throughout the run), it can reach high values locally, resulting for the total flow in an unsigned correlation coefficient ρ_C^A (equal to the sum of the absolute value of $\rho_C(\mathbf{x})$) of $\rho_C^A \approx 0.64$ at $t = 0$ and 0.56 at the final time for Run 2. All other runs with $\rho_C(t = 0) \approx 0$ behave in identical ways. In other words, nonlinearities in MHD are weaker than for neutral fluids, and thus MHD could turn out to be simpler than its fluid counterpart. It is not known whether a transition at high Reynolds number towards other type of attractors will occur.

In this context, a numerical simulation at the highest possible resolution will be of great use.

Furthermore, there are different interval of times during which the decay laws differ. The Kolmogorov-like phenomenology only deals with the intermediate temporal range of self-similar decay:

(i) after the initial transients have taken place, i.e. after the maximum enstrophy has been reached;
(ii) when viscous effects take place only because of inertial transfer to small scales, but with a Reynolds number still substantial;
(iii) before the effects of boundaries are felt owing to an inverse transfer to large scales.

The models developed in the spirit of Batchelor and based on the existence of a second invariant that undergoes inverse transfer (Hatori 1984; Biskamp 1994) cannot be ruled out by the present computations: sufficient scale separation at large scales much be achieved, in order to allow for both a k^s spectrum followed by the spectrum related to the inverse cascade to develop at the same time, together with a well-developed small-scale spectrum. Indeed, runs at a substantial Reynolds number must be performed, as shown by the present results, or otherwise the different models cannot be distinguished. This clearly awaits further study. We do observe some inverse transfer in all the flows reported here, with a change in the spectral slope of the large scales – a slope that thus cannot be controlled sufficiently, as the phenomenology ideally would require; this leads to a less satisfactory agreement with the model for the evolution of the integral scale (see below).

The decay law equivalent to the $(t-t_*)^{-10/7}$ of K41 for fluids is in MHD $E_{3D}^{(mhd)}(t) \sim (t-t_*)^{-5/6}$, in rough agreement with existing numerical data. However, Hossain et al. (1995) proposed a somewhat different phenomenology to model the energy decay. They concluded that, *both for fluids and for MHD*, $E(t) \sim (t-t_*)^{-1}$, a result backed up by 3D simulations at low resolution, which should be pursued at higher resolution to sort out fluid (K41-like) and MHD (IK-like) effects. Although 2D and 3D MHD are similar insofar as energy does cascade to small scales and there is a purely magnetic inverse cascade in both space dimensions, nevertheless the 3D case must also be analysed, in particular because the topological constraints due to magnetic helicity may alter the dynamical evolution of the flow; but this will require substantial resources.

A uniform magnetic field B_0 could have profound effects on the dynamical evolution as well. On the one hand, it is known to render the flow anisotropic (Shebalin et al. 1983), and an analysis in the spirit of that of Chasnov (1995) will be useful in that case. For a strong B_0, the first approximation to describe the resulting dynamics is to use the 2D MHD equations as studied here, in which case the IK phenomenology seems to prevail. A more realistic step will be to study the decay laws in the context of the reduced MHD equations (Montgomery 1982; Strauss 1993), including the four-wave formalism recently introduced by Ng and Bhattacharjee (1996). Note that when the uniform magnetic field is strong compared with the fluctuating fields, a weak turbulence formalism allows for the derivation of three-wave kinetic equations (Galtier et al. 1999; see also Galtier 1998). The exact analytical power-law solution to such equations leads to the absence of velocity–magnetic-field correlations to a $k_\perp^{-2}$

spectral law (where $k_\perp$ refers to the directions perpendicular to $\mathbf{B}_0$), and an ensuing slowing-down of the decay of the wave energy. This inertial law, steeper than its IK counterpart, was already postulated on dimensional grounds by Ng and Bhattacharjee (1997).

On the other hand, it is claimed (Cattaneo and Vainshtein 1991) that when $B_0 \neq 0$, small-scale turbulence is suppressed, and thus B_0 strongly alters the transport properties of turbulent fluids. Such claims are made in the framework of the dynamo problem (i.e. including a kinetic forcing term in order to obtain a growth of the magnetic field), which *stricto sensu* does not apply here, although the analysis extends as well to the decay problem, since it concerns the evaluation of transport coefficients. However, both the Kolmogorov and IK phenomenologies do *not* make explicit use of transport coefficients, but simply use dimensional constraints and the persistence of large-scale eddies. The unravelling of the effects of both the large-scale turbulent magnetic field and of a uniform component – using numerical simulations at high resolutions for long times and scanning parameter space thoroughly – can be done in 2D. The incorporation in a crude way in our model of such a strong slowing-down of energy transfer through the parameter $g \neq 4$ in (6) leads to decay laws that are measurably slower than what we actually observe in all cases studied here. For example, with $\tau_{\rm tr} = \tau_{NL}(\tau_{NL}/\tau_A)^2$ (for $g = 5$), one finds a $(t-t_*)^{-4/7}$ energy decay rate in 2D, substantially slower than any of the results of Table 1. This indicates that, in the framework of the model presented here, the standard IK phenomenology stands out, because it predicts the right amount of slowing-down of transfer. Note that in the presence of a non-zero uniform magnetic field, periodic boundary conditions may have to be dropped because of spurious reconnection effects (Berger 1995).

The weaker agreement between the model and the numerical data concerning the integral scale (by opposition to the energy) is probably due to the fact that the integral scale is more sensitive than the energy to the precise form of the energy spectrum at low wavenumber. The spectra with the chosen value for the peak wavenumber of the initial conditions $k_I = 10$ (somewhat low) are not entirely self-preserved, because of the inverse transfer of magnetic potential, and hence present a double spectral slope in the large scales, as can be seen for example in Fig. 4. Our choice of k_I represents a compromise, and more runs will have to be performed if one wishes to assess further the validity of decay models for MHD flows.

One firm conclusion can be drawn from the present parametric study, in agreement with other numerical results in the incompressible case (Biskamp 1994; Kinney et al. 1995; Hossain et al. 1995; Ting et al. 1986; Politano et al. 1995) as well as for supersonic conducting flows (Gammie and Ostriker 1996; MacLow et al. 1998): the decay in MHD is slower than for neutral fluids. We find that, moreover, this decay can be modelled in the spirit of the phenomenology of Kolmogorov based on the preservation of large-scale eddies together with an evaluation of energy transfer to small scales that takes into account in a simple way the presence of Alfvén waves, i.e. a way that acknowledges the fact that a large-scale magnetic field alters the dynamics, rendering it, to some degree, non-local as far as mode coupling is concerned, and locally (in space) anisotropic. The IK phenomenology encompasses in any dimension this slower decay, and as such is valuable. It seems to work as well

in the supersonic case for MHD; this can be attributed to the rigidity of the medium due to B_0 (taken here as either a uniform or a large-scale magnetic field), and to the presence of waves induced by B_0. Concerning the problem of interactions between waves and turbulence, it would be of interest to investigate the temporal scaling laws in MHD including dispersive terms, for example with an ambipolar drift term that arises for a low degree of ionization (as in the interstellar medium at large), or with the Hall current that appears in a generalized Ohm's law at high ionization (such as in the vicinity of protostellar jets or in the magnetosphere), or by considering electron MHD (Mandt et al. 1994), in which thin magnetic current sheets develop (Biskamp et al. 1995). These would be valuable first steps towards an evaluation of more complex plasma flows that include kinetic effects.

A precise understanding of the mechanisms at work for the decay of energy in a turbulent flow eludes us presently, and in fact many models can be envisaged that agree with experiments (see this review in Monin and Yaglom 1975, Sec. 16). In that light, there is a need to obtain and analyse higher-Reynolds-number data sets, including in two dimensions. These mechanisms are likely to be complex, if one is to draw an analogy with the case of the Burgers equation (see Gurbatov et al. 1997, and references therein), for which an exact solution is known via the Hopf–Cole transformation. However, what the several works on the Burgers equation show is that the persistence of large-scale eddies on which the phenomenology presented here relies, following Howarth, von Kármán and Kolmogorov, is the key ingredient of an understanding of decay laws in turbulent flows. Clearly the Kolmogorov expression for energy transfer does not work in MHD, and the IK evaluation $\epsilon_4 = z^4/lB_0$, if not exactly true, is nevertheless appropriate.

Finally, we note that a $(t-t_*)^{-1}$ law also obtains for stratified flows (Kimura and Herring 1995) and is attributed to a similar slowing-down of nonlinear transfer. In this context, one should recall that in both cases the formation of vorticity filaments is impeded; is the larger energy decay in isotropic neutral fluids linked to the instability (bursting) of these filaments? Then, if filaments were to disappear at high Reynolds numbers, should the decay law be modified as well? These points could be checked by experiments.

Acknowledgements

We are grateful to J. Herring for clarifying remarks at the onset of our work, and to him and R. Kerr for mentioning to us the unpublished result of G. S. Patterson concerning the t^{-2} decay law for Navier–Stokes flows.

Computations for the one-dimensional runs have been performed using the facilities provided by the programme 'Simulations Interactives et Visualisation en Astronomie et Mécanique (SIVAM)'; the C98 and the T3E at IDRIS (Orsay) were used in the two-dimensional configuration. This work has received partial financial support from CNRS (SDU) through Contract GdR-1202 MFGA.

Appendix. The influence of velocity–magnetic-field correlations

The phenomenology proposed in this paper can be further extended to include the effect of correlations between the velocity and the magnetic field by the introduction of a third parameter δ (see below). This results in the prediction of

an increasing difference between the decay rates of the $z^{\pm}$ energies as the correlation increases, as observed numerically (see Fig. 10a).

One now has to distinguish (Dobrowolny et al. 1980) between the $E^{\pm}(k)$ spectra and the temporal evolution of the $E^{\pm}(t)$ energies with their decay and transfer rates $\epsilon^{\pm}(t) = -\dot{E}^{\pm}(t)$, to take into account the possible asymmetry of the initial conditions for the $\mathbf{z}^{+}$ and $\mathbf{z}^{-}$ variables, leading to a non-zero mean correlation coefficient ρ_C between the velocity and the magnetic field. The relation (6) is then replaced by

$$\epsilon_g^{+} = \frac{(z^{+})^2}{\tau_{\rm tr}^{+}} = \frac{(z^{+})^2 (z^{-})^{g-2}}{l_B^{+} B_0^{(g-3)}}, \tag{A 1}$$

with a similar expression for ϵ_g^{-} using the $\pm$ symmetry of the MHD equations. Note that $g = 4$ and $l_B^{+} \sim l_B^{-}$ lead to $\epsilon_4^{+} \sim \epsilon_4^{-} \sim \epsilon_4$, and the relation (6) is recovered. At large scales, the spectra are assumed to behave as

$$E^{\pm}(k) \sim k^{s^{\pm}} \tag{A 2}$$

up to $k_B^{\pm} = 2\pi/l_B^{\pm}$, with $l_B^{\pm}$ being identified with the integral scales of the $\pm$ energies. The self-similar temporal evolutions of the energies and integral scales are taken as usual to be of the forms

$$z^{\pm\,2} \sim (t - t_*)^{-\alpha_{g,s}^{\pm}}, \qquad l_B^{\pm} \sim (t - t_*)^{\beta_{g,s}^{\pm}}. \tag{A 3}$$

Proceeding as before, this approach leads to $\alpha_{g,s}^{\pm} = (s^{\pm} + 1)\beta_{g,s}^{\pm}$ and

$$\beta_{g,s}^{\pm} = \frac{2[(g-2)(s^{\mp}+1) - 2]}{h(g)}, \tag{A 4a}$$

$$h(g) = (g-2)^2 (s^{+}+1)(s^{-}+1) - 4, \tag{A 4b}$$

for $h(g) \neq 0$. When $h(g) = 0$, one is led back to the uncorrelated case $s^{+} = s^{-} = s$ with $s = 2/(g-2)$, which gives

$$\alpha_{g,s}^{+} = \alpha_{g,s}^{-} = \alpha_{g,s} = \frac{1}{g-2}, \qquad \beta_{g,s}^{+} = \beta_{g,s}^{-} = \beta g, \qquad s = \tfrac{1}{2}.$$

In the case of negligible correlations, the decay laws (8), whatever the value of g, are recovered if and only if $s^{+} = s^{-}$, i.e. when the $z^{\pm}$ eddies behave in the same way.

The influence of the correlations between the velocity and magnetic field can be studied through the departure of the above temporal exponents from the $\alpha_{g,s}$ and $\beta_{g,s}$ obtained for the uncorrelated regime. Let us assume that

$$s^{\pm} = s \pm \delta, \tag{A 5}$$

with δ a positive parameter; note that $\delta = 0$ corresponds to the zero-correlation case. Writing

$$\alpha_{g,s}^{\pm} = \alpha_{g,s} \mp X_{g,s}^{\pm}(\delta), \qquad \beta_{g,s}^{\pm} = \beta_{g,s} \mp Y_{g,s}^{\pm}(\delta) \tag{A 6}$$

and taking $g = 4$, for simplicity, one obtains the following expressions:

$$X_{4,s}^{\pm}(\delta) = \frac{\delta(s + 2 \pm \delta)}{(s+2)[s(s+2) - \delta^2]}, \tag{A 7a}$$

$$Y_{4,s}^{\pm}(\delta) = X_{4,s}^{\mp}(\delta). \tag{A 7b}$$

These are all positive functions, since s is positive. Their derivatives with δ are also positive functions, and so $X^{\pm}_{4,s}(\delta)$ are increasing functions of δ. This means that $\alpha^{+}_{4,s}$ decreases as the parameter δ increases, while $\alpha^{-}_{4,s}$ increases. Assuming $\rho_C > 0$, this approach predicts a slower decay for z^{+^2} and a slower increase for l^{+}_{B} as the effect of growing velocity–magnetic-field correlations is modelled through $\delta > 0$. The opposite behaviour is obtained for z^{-2} and l^{-}_{B}. This is in qualitative agreement with the numerical results given in Sec. 4.1.5 for the temporal evolution of the $\pm$ energies and integral scales.

Of course, exchanging the signs between the $\pm$ quantities amounts to exchanging these behaviours between the z^{+} and z^{-} variables, i.e. exchanging the sign of the global correlation coefficient preserving the $\pm$ symmetry of the primitive MHD equations.

Finally, we note that, obviously, at maximum correlation, corresponding to pure Alfvén waves $\mathbf{v} = \pm\mathbf{b}$, nonlinearities are eliminated and the model presented in this paper, relying on nonlinear transfer, does not apply to this extreme case.

References

Bartello, P. and Warn, T. 1996 *J. Fluid Mech.* **326**, 357.

Batchelor, G. 1969 *Phys. Fluids* **12**, 233.

Berger, M. 1995 In: *Small-Scale Structures in Fluids and MHD* (ed. M. Meneguzzi, A. Pouquet and P. L. Sulem), p. 281. Lecture Notes in Physics, Vol. 462, Springer-Verlag, Heidelberg.

Biskamp, D. 1994 *Nonlinear Magnetohydrodynamics*, p. 196. Cambridge University Press.

Biskamp, D. and Welter, H. 1989 *Phys. Fluids* **B1**, 1964.

Biskamp, D., Schwarz, E. and Drake, J. F. 1995 *Phys. Rev. Lett.* **75**, 3850.

Brachet, M. E. 1990 *CR Acad. Sci. Paris* **311**, 375.

Burlaga, L. F. 1991 *J. Geophys. Res.* **96**, 5847.

Carbone, V. 1993 *Phys. Rev. Lett.* **71**, 1546.

Carnevale, G., McWilliams, J., Pomeau, Y., Weiss, J. and Young, W. 1991 *Phys. Rev. Lett.* **66**, 2735.

Carnevale, G., McWilliams, J., Pomeau, Y., Weiss, J. and Young, W. 1992 *Phys. Fluids* **A4**, 1314.

Cattaneo, F. and Vainshtein, S. 1991 *Astrophys. J.* **376**, L21.

Chasnov, J. 1995 *Phys. Fluids* **7**, 600.

Chasnov, J. 1997 *Phys. Fluids* **9**, 171.

Comte-Bellot, G. and Corrsin, S. 1966 *J. Fluid Mech.* **25**, 657.

Davidson, P. 1995 *J. Fluid Mech.* **299**, 153.

Dobrowolny, M., Mangeney, A. and Veltri, P. L. 1980 *Phys. Rev. Lett.* **45**, 144.

Dritschel, D. 1993 *Phys. Fluids* **A5**, 984.

Dudok det Wit, T. and Krasnosel'skihk, V. 1996 *Nonlinear Proc. Geophys.* **3**, 262.

Eyink, G. 1996 *Phys. Rev. Lett.* **77**, 2674.

Fournier, J. D., Sulem, P. L. and Pouquet, A. 1982 *J. Phys. A: Math. Gen.* **15**, 1393.

Frisch, U. 1995 *Turbulence: The Legacy of Kolmogorov*. Cambridge University Press.

Frisch, U., Pouquet, A., Sulem, P. L. and Meneguzzi, M. 1983 *Méc. Théor. Appl.* **2**, 191.

Fyfe, D. and Montgomery, D. 1976 *J. Plasma Phys.* **16**, 181.

Fyfe, D., Montgomery, D. and Joyce, G. 1977 *J. Plasma Phys.* **17**, 369.

Galtier, S. 1998 Turbulence et intermittence en magnétohydrodynamique: application à la couronne solaire. Thèse de l'Université de Grenoble I.

Galtier, S., Politano, H. and Pouquet, A. 1997 *Phys. Rev. Lett.* **79**, 2807.

Galtier, S., Gomez, T., Politano, H. and Pouquet, A. 1998 In: *Advances in Turbulence VII* (ed. U. Frisch), pp. 453–456. Kluwer, Dordrecht.

Galtier, S., Nazarenko, S., Newell, A. and Pouquet, A. 1999 To appear in a volume edited by T. Passot and P. L. Sulem, and published by Springer-Verlag.

Gammie, C. and Ostriker, E. 1996 *Astrophys. J.* **466**, 814.

Garnier, M., Alemany, A., Sulem, P. L. and Pouquet, A. 1981 *J. Méc.* **20**, 233.

Grappin, R., Pouquet, A. and Léorat, J. 1983 *Astron. Astrophys.* **126**, 51.

Grauer, R., Krug, J. and Marliani, C. 1994 *Phys. Lett.* **195A**, 335.

Grossman, S. and Lohse, D. 1991 *Phys. Rev. Lett.* **67**, 445.

Gurbatov, S., Simdyankin, S., Aurell, E., Frisch, U. and Tóth, G. 1997 *J. Fluid Mech.* **344**, 339.

Hatori, T. 1984 *J. Phys. Soc. Japan* **53**, 2539.

Heiles, C., Goodman, A. A., McKee, C. F. and Zweibel, E. G. 1993 In: *Protostars and Planets III* (ed. E. H. Levy and J. I. Lunine), p. 279. University of Arizona Press, Tucson.

Hossain, M., Gray, P., Pontius, D., Matthaeus, W. and Oughton, S. 1995 *Phys. Fluids* **7**, 2886.

Iroshnikov, P. 1963 *Soviet Astron.* **7**, 566.

Kerr, R. 1981 Theoretical investigation of a passive scalar such as temperature in isotropic turbulence. PhD thesis, Cornell University.

Kida, S. 1979 *J. Fluid Mech.* **93**, 337.

Kimura, Y. and Herring, J. 1995 In: *Small-Scale Structures in Fluids and MHD* (ed. M. Meneguzzi, A. Pouquet and P. L. Sulem), p. 195. Lecture Notes in Physics, Vol. 462, Springer-Verlag, Heidelberg.

Kinney, R., McWilliams, J. C. and Tajima, T. 1995 *Phys. Plasmas* **2**, 3623.

Kolmogorov, A. 1941 *Dokl. Akad. Nauk SSSR* **31**, 538.

Kraichnan, R. H. 1965 Phys. Fluids **8**, 1385.

Kraichnan, R. H. and Montgomery, D. 1980 *Rep. Prog. Phys.* **43**, 547.

Léorat, J., Passot, T. and Pouquet, A. 1990 *Mon. Not. R. Astron. Soc.* **243**, 293.

Lesieur, M. and Schertzer, D. 1978 *J. Méc.* **17**, 609.

Lohse, D. 1994 *Phys. Rev. Lett.* **73**, 3223.

MacLow, M.-M., Klessen, R., Burkert, A. and Smith, M. 1998 *Phys. Rev. Lett.* **80**, 2754.

Mandt, M. E., Denton, R. E. and Drake, J. F. 1994 *Geophys. Res. Lett.* **21**, 73.

Matthaeus, W. H. & Goldstein, M. L. 1982 *J. Geophys. Res.* **87A**, 6011.

Matthaeus, W. and Montgomery, D. 1980 *Ann. NY Acad. Sci.* **357**, 253.

Matthaeus, W. and Montgomery, D. 1984 In: *Statistical Physics and Chaos in Fusion Plasmas* (ed. C. W. Horton and L. E. Reichl), p. 297. Wiley, New York.

Meneguzzi, M., Politano, H., Pouquet, A. and Zolver, M. 1996 *J. Comput. Phys.* **123**, 32.

Moffatt, H. K. 1967 *J. Fluid Mech.* **28**, 571.

Monin, A. and Yaglom, A. 1975 *Statistical Fluid Mechanics*, Vol. II MIT Press, Cambridge, MA (translated from the Russian: Nauka, Moscow, 1965).

Montgomery, D. 1982 *Physica Scripta* **T2/1**, 83.

Ng, C. S. and Bhattacharjee, A. 1996 *Astrophys. J.* **465**, 845.

Ng, C. S. and Bhattacharjee, A. 1997 *Phys. Plasmas* **4**, 605.

Nore, C., Brachet, M. E., Politano, H. and Pouquet, A. 1997 *Phys. Plasma Lett.* **4**, 1.

Oughton, S., Priest, E. and Matthaeus, W. 1994 *J. Fluid Mech.* **280**, 95.

Passot, T., Politano, H., Pouquet, A. and Sulem, P. L. 1990 *Theor. Comput. Fluid Dyn.* **1**, 47.

Politano, H. and Pouquet, A. 1995 *Phys. Rev.* **E52**, 636.

Politano, H., Pouquet, A. and Sulem, P. L. 1989 *Phys. Fluids* **B1**, 2230.

Politano, H., Pouquet, A. and Sulem, P. L. 1995 In: *Small-Scale Structures in Fluids and*

MHD (ed. M. Meneguzzi, A. Pouquet and P. L. Sulem), p. 281. Lecture Notes in Physics, Vol. 462, Springer-Verlag, Heidelberg.

Politano, H., Pouquet, A. and Carbone, V. 1998 *Europhys. Lett.* **43**, 516.

Pouquet, A. 1978 *J. Fluid Mech.* **88**, 1.

Pouquet, A. 1993 In: *Les Houches XLVII: Astrophysical Fluid Dynamics* (ed. J. P. Zahn and J. Zinn-Justin), p. 139, Elsevier, Amsterdam.

Saffman, P. 1967a *Phys. Fluids* **10**, 1349.

Saffman, P. 1967b *J. Fluid Mech.* **27**, 581.

She, Z. S. and Leveque, E. 1994 *Phys. Rev. Lett.* **72**, 336.

Shebalin, J., Matthaeus, W. and Montgomery, D. 1983 *J. Plasma Phys.* **29**, 525.

Smith, M., Donnelly, R., Goldenfeld, N. and Vinen, W. 1993 *Phys. Rev. Lett.* **71**, 2583.

Strauss, H. 1993 *Geophys. Res. Lett.* **20**, 325.

Stribling, T., Matthaeus, W. H. and Gosh, S. 1994 *J. Geophys. Res.* **99**, 2567.

Ting, A., Matthaeus, W. and Montgomery, D. 1986 *Phys. Fluids* **29**, 3261.

Thomas, J. 1968 *Phys. Fluids* **11**, 1245.

Thomas, J. 1970 *Phys. Fluids* **13**, 1877.

Vainshtein, S. and Cattaneo, F. 1992 *Astrophys. J.* **393**, 165.

Warhaft, Z. and Lumley, J. 1978 *J. Fluid Mech.* **88**, 659.

Yanase, A. 1997 *Phys. Plasmas* **4**, 1010.